A Multi-Sensor Passive Occupant Localization

Murat Ambarkutuk

Dissertation submitted to the Faculty of the
Virginia Polytechnic Institute and State University
in partial fulfillment of the requirements for the degree of

Doctor of Philosophy
in
Computer Engineering

Paul E. Plassmann, Chair
Creed F. Jones, Co-chair
A. Lynn Abbott
Almuatazbellah Boker
Zhenhua Tian
Sa'ed A. Alajlouni

September 27, 2024
Blacksburg, Virginia

Keywords: Occupant Tracking, Footstep Localization, Uncertainty Quantification,
Accelerometer Sensor Networks, Byzantine Sensor Elimination

A Multi-Sensor Passive Occupant Localization

Murat Ambarkutuk

(ABSTRACT)

Indoor localization has emerged as a critical technology for enhancing the functionality and efficiency of smart environments. This dissertation focuses on vibro-localization, a novel IOL methodology that determines occupant positions by analyzing floor vibrations caused by footfall patterns. Unlike traditional localization techniques that rely on visual or radio-based sensing, vibro-localization leverages accelerometers fixed to the floor to capture vibro-measurements, offering a cost-effective and privacy-preserving alternative. The primary objective of this research is to address significant limitations in existing vibro-localization approaches, including sensor imperfections, measurement uncertainty, and complex wave dynamics. To this end, we develop comprehensive models that characterize both random and systematic errors introduced by accelerometers, integrating these models into the localization framework to enhance accuracy. Furthermore, we quantify the uncertainty in vibro-measurements and elucidate their contribution to localization errors, providing a robust foundation for error mitigation strategies. A key contribution of this work is the introduction of an information-theoretic Byzantine Sensor Elimination (BSE) algorithm. This algorithm assesses the reliability of vibro-measurement vectors by categorizing sensors into consistent and divergent subsets, thereby minimizing the

impact of external uncertainties such as reflections and dispersion. Additionally, we propose multi-sensor vibro-localization techniques that aggregate data from multiple accelerometers, enhancing robustness against individual sensor inaccuracies and environmental variabilities. To accurately model wave propagation, this dissertation advances parametric models that account for dispersion, attenuation, and material inhomogeneities in the floor structure. These models facilitate precise occupant localization even with low-spectral resolution in transfer function estimates. Empirical validation using controlled experimental data demonstrates significant improvements in localization accuracy and precision over baseline methods, highlighting the efficacy of the proposed techniques. The outcomes of this research contribute to the development of economically feasible and ethically sound IOL technologies, broadening their applicability across various domains such as smart homes, healthcare, and energy management. By addressing critical challenges in sensor reliability and wave dynamics, this dissertation paves the way for more accurate, reliable, and scalable indoor localization systems.

A Multi-Sensor Passive Occupant Localization

Murat Ambarkutuk

(GENERAL AUDIENCE ABSTRACT)

In our increasingly connected world, knowing the precise location of individuals within indoor spaces—such as homes, offices, and hospitals—has become essential for enhancing convenience, safety, and energy efficiency. Traditional methods for indoor localization often rely on cameras or radio signals, which can be expensive and raise privacy concerns. This dissertation introduces an innovative approach called vibro-localization, which determines the position of occupants by analyzing the subtle vibrations in the floor caused by their footsteps. Vibro-localization utilizes simple and affordable sensors called accelerometers, which are placed on the floor to detect vibrations. When a person walks, their footsteps generate unique vibration patterns that travel through the building structure. By capturing and analyzing these patterns, our system can accurately pinpoint the individual's location without the need for invasive cameras or constant radio signal transmissions. This method not only reduces costs but also preserves the privacy of occupants, as it does not capture visual or personal data. One of the main challenges in vibro-localization is ensuring accuracy despite various sources of error. Sensors can introduce noise and inaccuracies, and factors like the building's materials and layout can affect how vibrations propagate. To overcome these challenges, this research develops sophisticated models

that account for sensor imperfections and environmental factors. By understanding and correcting for these variables, the system can deliver precise location data even in complex indoor environments. A significant advancement presented in this work is the development of an algorithm that intelligently selects the most reliable sensor data. This algorithm distinguishes between consistent measurements and those affected by external disturbances, such as echoes or structural inconsistencies, ensuring that only the highest quality data is used for localization. This not only improves accuracy but also makes the system more robust and reliable in real-world settings. Moreover, the dissertation explores the use of multiple sensors working together to enhance localization performance. By combining data from several accelerometers, the system can cross-verify measurements and reduce the impact of individual sensor errors. This multi-sensor approach leads to more stable and accurate location tracking, making the technology suitable for a wide range of applications. To validate the effectiveness of the proposed vibro-localization techniques, extensive experiments were conducted in controlled environments. The results demonstrated significant improvements in both accuracy and reliability compared to existing methods, showcasing the potential of vibro-localization as a practical solution for indoor positioning needs. The implications of this research are far-reaching. In smart homes, vibro-localization can enable automated lighting and climate control based on occupant presence, enhancing energy efficiency and comfort. In healthcare settings, it can assist in monitoring patient movements, ensuring safety and improving care. Additionally, in emergency situations, accurate indoor localization can facilitate quicker and more efficient evacuations. In summary, this dissertation presents a ground-

breaking approach to indoor localization that is cost-effective, privacy-preserving, and highly accurate. By leveraging floor vibrations and advanced sensor data processing techniques, vibro-localization offers a viable alternative to traditional methods, with broad applications that can significantly enhance the functionality and safety of indoor environments. This research not only addresses current limitations in indoor localization technology but also paves the way for future innovations in smart building systems and occupant-aware technologies.

Dedication

To my beloved wife, Zeynep;

to my prince χ;

to my parents and sister...

Acknowledgments

I would like to express my deepest gratitude to my advisor, Dr. Plassmann, and my co-chair, Dr. Jones, for their unwavering support and guidance throughout my doctoral journey. Their expertise and mentorship have been invaluable. My sincere appreciation goes to my committee members—Dr. Abbott, Dr. Boker, Dr. Tian, and Dr. Alajlouni—for their valuable feedback and insights, which have greatly enhanced the quality of this work. To my beautiful wife, Zeynep, and my prince, χ, as well as my parents and sister: thank you for your endless love and encouragement. Your support has been my foundation. I am grateful to the Bradley Department of Electrical and Computer Engineering and Mechanical Engineering for providing the resources and opportunities that made this research possible. A special thanks to my previous advisor, Pablo Tarazaga, and his group (VAST and FAST) for their initial guidance and camaraderie, which set me on this path. To my friends and colleagues, your support and collaboration have been instrumental in this journey. Thank you for standing by me. Finally, I acknowledge Space@VT, ICAT, CNRE, MLSoC, and the entire Virginia Tech community for fostering an environment I have proudly called home for the last decade.

Contents

List of Figures

List of Tables

Acronyms

BSE Byzantine Sensor Elimination

CDF Cumulative Distribution Function

FoV Field-of-View

HMM Hidden Markov Model

IOL Indoor Occupant Localization

LOTUS Law of the Unconscious Statistician

MAD Mean Absolute Deviation

MLE Maximum Likelihood Estimation

MOCAP Motion Capture

PDF Probability Density Function

PFEEL Probabilistic Force Estimation and Event Localization

RMSE Root Mean Squared Error

SNR Signal-to-noise Ratio

SONAR Sound Navigation and Ranging

TDoA Time-Difference-of-Arrival

ToA Time-of-Arrival

ToI Target of Interest

Chapter 1

Introduction

Target localization refers to determining the position of a specific entity or an object, or commonly known as Target of Interest (ToI) in a fixed space. In the context of Indoor Occupant Localization (IOL), the ToIs are the occupants and the space is the indoor environment, such as a building or room. By employing an IOL technology, an interface between the occupants and the building is established [12, 61]. This interface can be used in numerous applications, such as energy management by adjusting heating or cooling based on occupancy [14, 30, 56], ensuring safety during emergency evacuations, monitoring patient movements in healthcare settings, or enhancing personalized experiences in smart homes.

However, there are also significant concerns related to IOL such as privacy, cost and accuracy to name a few. The primary among these is the issue of privacy. As occupants are continuously tracked, there is a risk of misuse of this data or unauthorized malicious access, potentially revealing sensitive information about an individual's habits, routines, or health conditions. Additionally, there may be discomfort among users in being constantly monitored, leading to feelings of surveillance.

The choice of sensing methodology employed in an indoor localization also plays a

pivotal role in the prospect of the localization outcomes. Visual sensing modality, for example, have gained popularity in the realm of IOL due to their accuracy and ability to provide rich contextual information. However, these systems often come with an exceptionally high cost. The main reason for this drawback is that the cameras are limited by their Field-of-View (FoV); thus, many of them need to be deployed to cover the localization space. This not only increases the initial investment for setting up such systems but can also inflate the ongoing maintenance and upgrade costs.

Figure 1.1 illustrates a comparison between different sensing modalities frequently employed in occupant localization systems. Overall, such sensor modalities fall under two sensing schemes: active and passive. The latter relies on the measurements of the ambient space to deduce the occupant location by tracking the changes in the localization space. Therefore, these techniques do not rely on special beacons, known features, etc to track across the localization space. For instance, visual, acoustic and vibration sensing are generally examples of passive schemes. On the other hand, the active schemes require occupants to carry a special feature that can be recognized by the localization system. In other words, the detection and localization of the occupant often conducted by tracking such known features in the space. Therefore, active perception schemes tend to yield more accurate and precise estimations about the occupant's location. Motion Capture (MOCAP) is an example of such localization systems where the occupants carry special reflecting markers and the localization space is illuminated with special sources that emit light modulated at a specific frequency. The occupants are localized by tracking the reflections with multiple cameras tuned to detect only the modulated light. The use

of such knowledge manifets itself as increased localization accuracy and precision.

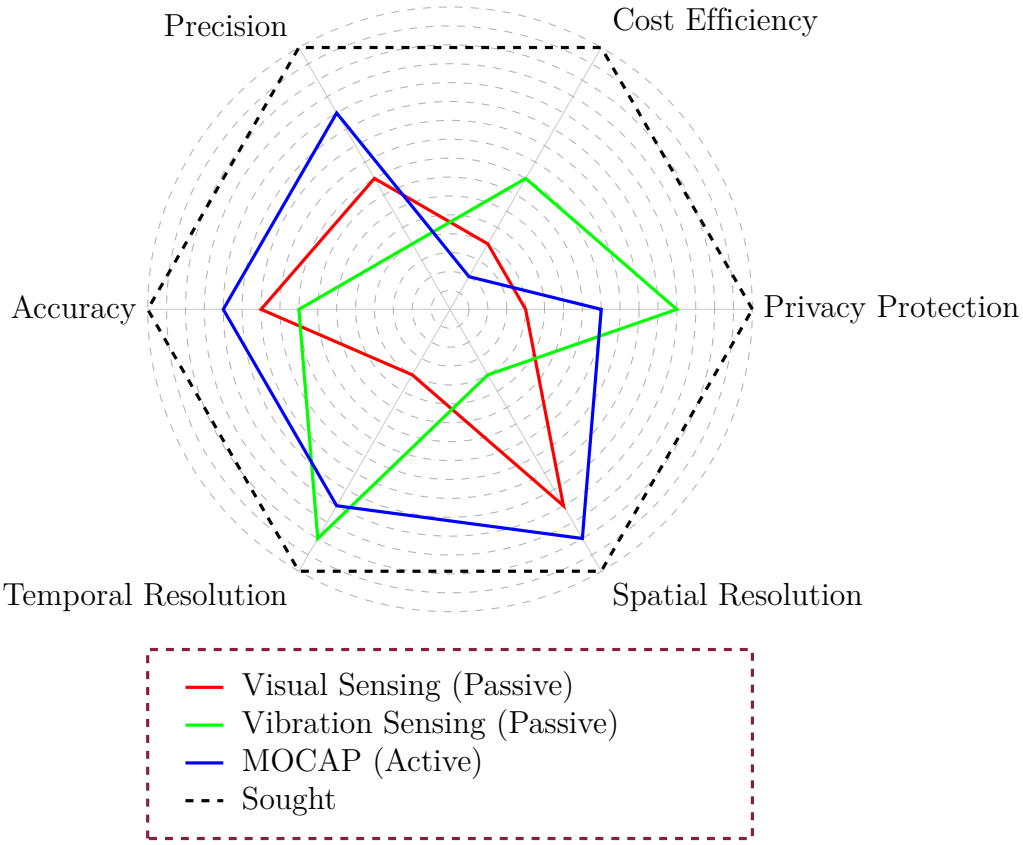

Figure 1.1: A visual comparison of three popular sensing schemes used in occupant localization.

This document provides a deep look into existing IOL techniques and proposes a new approach that does not require expensive sensors and infringe upon occupants' privacies. Aiming to make IOL both economically feasible and ethically sound, our approach seeks to democratize access to localization technologies, ensuring a broader spectrum of applications without compromising individual rights.

This dissertation proposal serves as a comprehensive blueprint for the forthcoming

research on IOL. It encapsulates the work carried out thus far, laying a solid foundation for the scholarly discourse. The primary goal of this document is to provide the research trajectory, detailing the methodological approaches, theoretical frameworks, and empirical inquiries undertaken. Furthermore, this proposal aims to provide a clear roadmap for what lies ahead, outlining the steps that will lead to the culmination of a dissertation. By presenting both the groundwork already established and the tentative future directions, this proposal seeks to offer a holistic view of the research activities, ensuring clarity, coherence, and rigor in the pursuit of the insights into IOL.

1.1 Literature Review

Structural vibration-based occupant localization is a perception methodology where occupants' locations in an indoor environment are determined by analyzing the floor vibrations due to their footfall patterns. Specifically, these methods employ the measurements of accelerometers that are fixed to the floor. Henceforth, the terms vibro-localization and vibro-measurements will refer to such localization techniques and the measurements used in these techniques, respectively. Vibro-localization techniques facilitate a myriad of applications ranging from smart home monitoring and event classification [16, 35, 59] to human gait assessment [18, 24, 32, 33] and occupant identification and tracking [23, 26, 31, 51, 53].

Energy-based vibro-localization techniques utilize the energy that is inherent in vibro-measurements as a localization feature because the signal energy serves as a

consistent metric for gauging the magnitude of the vibro-measurements [6, 19, 39, 57]. Specifically, higher signal amplitudes result in larger energy values registered by the sensors, and vice versa. By employing this notion, energy-based vibro-localization techniques characterize the relationship between the signal energy and the length of the propagation path. Therefore, these techniques offer a simplified approach to occupant localization, thereby reducing the need for exhaustive signal analysis. In this study, the terms signal energy, power, intensity, and strength are used interchangeably despite their nuanced differences.

Dispersion is a natural phenomenon where different frequency components of structural waves propagate at different velocities in the medium, i.e., the floor. This phenomenon has been seen as one of the major contributors to localization errors; hence, substantial scholarly endeavors have been directed toward examining the floor's dispersive attributes on localization outcomes. These researchers have mitigated the dispersive effects inherent in the floor by isolating narrow frequency bands. These bands, derived via Continuous Wavelet Transformation, remain unaffected by dispersion [15, 34, 43, 54]. Kwon and Agha [34], for instance, presented a successful human activity recognition system utilizing floor vibro-measurements. Their technique employed a feature extraction step based on wavelet packet decomposition coupled with statistical measures to capture the unique characteristics of different activities. The empirical findings emphasized the efficacy of the proposed technique in the precise identification of diverse human activities. Racic et al. [54] presented a technique for the detection and classification of human activities via floor vibrations. They employed an approach involving a combination of wavelet-based feature

extraction and a support vector machine classifier to accurately identify different activities, demonstrating the potential of floor vibro-measurements for activity monitoring and recognition in smart environments. Such narrowband filtering essentially compromises the spatial resolution of the localization technique in hand; this challenge, especially in the context of radio-localization, has been discussed in detail (for instance, [28]).

The Warped Frequency Transformation technique has been also utilized to discern the dispersion curve, to mitigate perturbations attributed to dispersion [38, 58]. There exist system-theoretic techniques that characterize the dynamic behavior of the floor via transfer function estimation [17, 40, 48]. Additionally, the Green's function has been employed to account for wave reflections and its dispersion [49]. Despite their precision in empirical analyses, these techniques exhibit limitations in their capacity to generalize the complex material properties and boundary conditions inherent in floors.

On the other hand, Bahroun et al. [10] presented their work formalizing the group velocities, i.e., a major component of signal energy, as a function of propagation path distance. These promising results paved the way for the model-based techniques which tend to explain the wave phenomena from the data. Alajlouni et al. [5], for instance, showed their hypothesis of an energy-decay model (energy logarithmically decays with propagation distance) as a localization model. In their work, Pai et al. [50] analyzed whether a relationship exists between the occupant's footfall patterns and the measured signal characteristics in an empirical case study. In light of their work, the authors assert that there is no evidence of a monotonic relationship

between the amplitude or kurtosis of the measured signal and the propagation distance. Parametric energy-decay models highlight the exciting potential for further improvement [3, 4, 55, 60].

Along with parametric decay models, Poston et al. [52], in an alternative attempt, moved the localization frameworks to a probabilistic framework by modeling the probability of detection and false alarm. Alajlouni et al. [3] took a similar approach to localize the occupant by maximizing the sensor likelihood functions given the hypothesis of the sensor's time domain measurements and the energy-decay model proposed in their earlier work. Wu et al. [60] propose G-Fall, a device-free fall detection system based on floor vibrations collected by geophone sensors. Their system utilizes Hidden Markov Models (HMMs) and an energy-based vibro-localization technique, achieving precise and user-independent fall detection with a significant reduction in false alarm rates.

1.2 Limitations of the Previous Literature

One of the inherent challenges limiting the ability and success of vibro-localization techniques is that these techniques are single-shot estimators: each heel-strike and its corresponding vibro-measurement vector are unique; hence, repeated measurements for a single step are not easily attainable. Therefore, most of the common estimation frameworks cannot be directly employed in such localization systems. This challenge brings about the following limitations in the landscape of vibro-localization techniques:

C1. **Sensor Imperfections**: Accelerometers are not ideal and tend to introduce random and systematic errors in the vibro-measurement vector during signal acquisition. These sensor imperfections were not thoroughly characterized in existing literature, hindering a complete understanding of localization errors unless these errors are explicitly identified and integrated into vibro-localization frameworks.

C2. **Uncertainty in Measurement Errors**: The contribution of measurement errors to localization errors remains unclear. Specifically, sensing errors in vibro-measurements have yet to be directly linked to localization inaccuracies. Accounting for errors in the vibro-measurement vector is imperative for the success of localization techniques.

C3. **Information Reliability Assessment**: Beyond measurement imperfections, numerous uncertainty sources such as reflections and dispersion affect the reliability of energy-based vibro-localization techniques. To mitigate the adverse effects of unreliable sensor information, a metric is needed to assess the reliability of each vibro-measurement vector at any given time.

C4. **Non-Ideal Sensor Characteristics**: Measurement uncertainty significantly contributes to localization error. For example, assuming a normal distribution of signal energy measurements, as done by [3], may not hold in real-world settings due to the complex nature of wave propagation. This can result in gradient-based solvers failing to converge to the global optimum, leading to suboptimal localization outcomes.

C5. **Complex Wave Dynamics**: Wave propagation is influenced by factors like dispersion, attenuation, and material inhomogeneities. Simplistic assumptions, such as a constant wave speed [36, 37, 44] or wave speed solely dependent on propagation distance [10], fail to capture the intricate dynamics, potentially causing errors in localization accuracy.

C6. **Variability in Footsteps**: Ground reaction forces generated by footsteps vary based on individual gait characteristics, including step length, step width, and walking speed. This variability can introduce errors in localization results, as techniques may not accurately account for the unique features of each individual's footsteps.

C7. **Unknown Forcing Functions**: Accurate estimation of the force shape generated by occupants' footsteps is challenging due to dependencies on gait characteristics, floor material properties, and wave frequency. Inaccurate force estimation can lead to errors in modeling wave propagation, thereby affecting localization accuracy [17, 41, 42].

C8. **Rapid Propagation Relative to Sampling Rates**: Footsteps generate fast and repetitive signals, resulting in insufficient samples to capture wave characteristics effectively at reasonable sampling rates. This leads to low spectral resolution in transfer function estimates, as seen in approaches like [41]. Limited frequency resolution combined with measurement uncertainty can significantly degrade the accuracy of localization results.

1.3 Summary of the Contributions

This manuscript presents energy- and Time-Difference-of-Arrival (TDoA)-based vibro-localization techniques that address sensor imperfections and their effects on localization results. The proposed techniques employ a family of accelerometers placed on a floor to generate multiple vibro-measurement vectors across several steps. One of the proposed techniques incorporates two corrective steps during localization: (i) comprehensive uncertainty quantification to minimize internal errors during signal acquisition in the vibro-measurement vectors; and (ii) an information-theoretic BSE algorithm to mitigate external uncertainty sources such as reflections and dispersion.

The following points summarize the contributions of this work:

C1. **Advancing Single- and Multi-Sensor Vibro-Localization** (Addresses Limitations L1, L2 and Challenges 1): Chapter 2 provides a detailed study on uncertainties in energy-based vibro-localization techniques, covering both single-sensor and multi-sensor scenarios. This bridges a gap in existing research, which predominantly focuses on multi-sensor systems.

C2. **Analytical and Numerical Analysis of Localization Error** (Addresses Limitation L2): Chapter 2 employs theoretical methods (via PDF transformation theorem) and numerical techniques (Taylor Series expansion on the mean localization error with Law of the Unconscious Statistician (LOTUS)) to estimate the mean localization error, considering factors such as sensor noise and signal-to-noise ratio (SNR).

C3. **Comprehensive Uncertainty Quantification in Vibro-Localization** (Addresses Limitations L1, L2): The proposed vibro-localization technique in Chapter 3 utilizes an explicit error model for each sensor, enabling complete uncertainty quantification and minimizing localization errors due to measurement imperfections [8].

C4. **Information-Theoretic BSE Algorithm for Reliability Assessment** (Addresses Limitation L3): Chapter 3 introduces a BSE algorithm that categorizes sensors into consistent and divergent subsets using a greedy information-theoretic approach. This algorithm ensures a locally-optimal subset of sensors to minimize localization errors.

C5. **Multi-Sensor Perception for Robust Localization** (Addresses Challenge 1): We propose a multi-sensor technique that aggregates information from multiple sensors without assuming a normal distribution in signal energy measurements. Averaging during signature estimation enhances robustness to real-world complexities and variabilities.

C6. **Enhanced Wave Propagation Modeling** (Addresses Challenges 2, 3, and 4): We introduce a model-based approach that accurately captures dispersive and attenuative properties of structural vibration waves, focusing on key parameters such as wave speed and attenuation coefficient. This approach improves localization accuracy by avoiding oversimplifications inherent in previous models.

C7. **Parametric Approach to Modeling Physical Properties** (Addresses Chal-

lenge 5): We develop a piecewise constant velocity profile to model dispersion mechanisms, allowing occupant location estimation even with low-spectral resolution in transfer function estimates. Calibration of the vibro-localizer involves fitting the transfer function to measured waveforms by estimating wave velocity and attenuation coefficients.

C8. **Empirical Validation of Proposed Techniques** (Addresses Limitations L1–L3): We validate the proposed techniques using data from previously conducted controlled experiments [8], demonstrating significant improvements over baseline approaches [1] in terms of both accuracy and precision.

C9. **Quantification of Empirical Precision and Accuracy** (Addresses Limitation L3): Utilizing results from the empirical validation study, we quantify the empirical correlation between precision and accuracy achieved with the proposed vibro-localization technique. These correlation metrics provide deeper insights into the technique's performance and potential failure modes.

1.4 Outline

This proposal is organized into distinct chapters, each addressing essential aspects of indoor localization and the innovative use of sensor networks to measure floor vibrations. Below is the overall outline of the proposal:

- **Chapter 1: Introduction** This chapter sets the stage by outlining the primary challenges associated with localization in indoor environments. It estab-

lishes the significance of the research, its relevance in the current technological landscape, and introduces the reader to the broader context and objectives of the study.

- **Chapter 2: Quantification of Measurement Uncertainity**

  This chapter presents an in-depth examination of a unique vibro-localization technique. Emphasis is placed on its stochastic nature, the role of multi-sensor integration, and the novel concept of Byzantine sensor elimination. The methodology, experimental setup, results, and discussions pertaining to this technique are elaborated upon.

- **Chapter 3: A Multi-Sensor Stochastic Energy-based Vibro-localization Technique with Byzantine Sensor Elimination**

  This chapter presents an in-depth examination of a unique vibro-localization technique. Emphasis is placed on its stochastic nature, the role of multi-sensor integration, and the novel concept of Byzantine sensor elimination. The methodology, experimental setup, results, and discussions pertaining to this technique are elaborated upon.

- **Chapter 4: Modeling and Analysis of Dispersive Propagation of Structural Waves for Vibro-Localization**

  This chapter introduces a new technique that models the dispersive propagation of structural waves in the context of vibro-localization. The methodology, experimental setup, results, and discussions pertaining to this technique are elaborated upon.

- **Chapter 5: Conclusions and Future Work**

  This chapter provides our conclusions and future work based on the findings and insights gained from the research. It also outlines the potential directions for future research and the implications of the proposed techniques in the broader context of indoor localization.

Chapter 2

Energy-based Vibro-Localization Technique with Single Sensor

As motivated in the previous chapter, the uncertainty of vibro-measurements holds a significant role in the success of vibro-localization techniques. Prior work has attempted various methods to quantify and remedy the effects of errors contained in vibro-measurement vectors. There exist approaches attempting to remedy these errors in the vibro-localization context by employing Kalman filtering framework [2], Maximum Likelihood Estimation (MLE) [11], or sensor elimination methods [45] to minimize as small information as possible. While these frameworks multiple sensors to be employed to remedy the effects of error in vibro-measurement vectors, there is limited effort in the quantification of the vibro-localization errors when a single sensor is employed.

2.1 Introduction

In this chapter, we study the localization outcomes of an energy-based vibro-localization technique in which sensor disturbances of a single sensor such as sensor bias and noise govern the uncertainty of the location estimations. In order to study these errors, we employ different statistical methods to quantify the bounds of the mean and PDF of the vibro-localization errors.

Portions of the content covered in this chapter have been previously presented in [9]. This work has laid the groundwork for further research, particularly in the context of exploring the uncertainties inherent in localization estimations using accelerometer data. Building upon these foundational insights, the current dissertation extends the scope by delving deeper into the uncertainty of energy-based vibro-localization techniques, especially when dealing with a multi-sensor setup. The methodologies and findings from [9] have been instrumental in shaping the research approach and analysis presented in this chapter.

2.1.1 Summary of the Contributions

This chapter makes several key contributions to the field of vibro-localization, particularly in the context of single-sensor setups:

- **Comprehensive Methodological Framework**: Development and implementation of a rigorous statistical framework to quantify and analyze the errors in vibro-localization. This includes a novel approach to model sensor

measurement imperfections and their impact on localization accuracy.

- **Analytical and Numerical Analysis of Localization Error**: The chapter employs both theoretical and numerical methods to estimate the mean localization error, considering factors like sensor noise and signal-to-noise ratio (SNR).

- **Practical Insights for Vibro-Localization Systems**: The findings offer practical insights for the design and improvement of vibro-localization systems, highlighting the critical role of sensor noise and SNR in achieving accurate localization.

These contributions are expected to provide a foundation for future research in the field, particularly in enhancing the accuracy and reliability of vibro-localization systems in practical applications.

2.1.2 Outline

This chapter focuses on the uncertainties in single-sensor energy-based vibro-localization techniques. The structure of the chapter is as follows:

1. Section 2.1 introduces the context and significance of vibro-measurement uncertainties in vibro-localization, reviewing prior work and establishing the main focus of the chapter.

2. Section 2.2 lays the foundational definitions for the study, including localization space, sensor measurements, and the concept of vibro-measurement vector energy.

3. Section 2.3 presents the methodology for quantifying and analyzing errors in single-sensor vibro-localization, including the development of the Parametric Energy Decay Model and the derivation of the PDF of localization error.

4. Section 2.4 conducts a parametric study to examine the impact of sensor noise and SNR on localization accuracy, employing theoretical and empirical analyses.

5. Section 2.5 summarizes the key findings, emphasizing the influence of sensor noise and SNR on vibro-localization accuracy and the effectiveness of the applied analytical methods.

2.2 Problem Definition

In this study, we consider a single sensor energy-based vibro-localization technique to localize an occupant in an indoor environment. This localization technique can be considered as an elemental building-block for much larger vibro-localization techniques. Therefore, understanding the error characteristics of such localization techniques will reveal how to improve complex vibro-localization techniques.

To formally state the localization problem in hand, we put forward a set of definitions such the localization space, sensor's measurement ability, etc. The localization space

$\mathcal{S}$ is a bounded area in a building which contains both the occupant and sensor.

Definition 2.1 (Occupant and Localization Space $\mathcal{S}$)**.** Localization space $\mathcal{S}$ is a closed subset of a building which contains a sensor tracking a dynamic occupant. In other words, the localization space $\mathcal{S}$ is a set of points that an occupant can reside, and is defined with respect to the sensor.

An occupant within the context of this study refers to a dynamic and non-evasive target residing in the localization space $\mathcal{S}$. The dynamic nature of the occupant implies movement or potential for movement within the confines of $\mathcal{S}$, and the term "non-evasive" denotes that the occupant's behavior is not intentionally altering to avoid detection or localization. The occupant's presence and movement are key factors influencing the sensor measurements, and thus, they are critical to the accuracy and effectiveness of the vibro-localization technique.

With the definition of localization space $\mathcal{S}$, we can define an event with which the occupant is localized.

Definition 2.2 (Event: Footstep)**.** An event, specifically a footstep, is characterized as a distinct occurrence within the localization space $\mathcal{S}$ that can be identified by sensor measurements. The localization events are phenomena that results some changes in the localization space $\mathcal{S}$. Within a set of time-steps $\mathcal{K} = \{1, \ldots, n_k\}$, a footstep event is represented by a unique pattern in the sensor data that corresponds to the physical act of an occupant taking a step.

The measured data often exhibit a sharp, impact-like waveform, akin to a blip on a Sound Navigation and Ranging (SONAR) screen. This waveform is characterized

by a sudden onset that overcomes the ambient noise, followed by a rapid decay that diminishes quickly below the surrounding ambient noise. This pattern is discernible from other ambient sensor readings due to its distinctive signal characteristics, which include amplitude, duration, and frequency. The identification and analysis of these footsteps are crucial for the precise localization of the occupant within $\mathcal{S}$. Considering each event results in unique perturbations and a set of sensors observing them in the ambient space, our task is to distinguish ToI from the background and provide an estimated location vector $\hat{\mathbf{x}}$ corresponding to it.

In this study, the measurements of a single accelerometer are used to localize the occupant. In order to derive the localization problem, we put forward a model for the sensor measurements as given in Definition 2.3.

Definition 2.3 (Sensor Measurement)**.** Let $\hat{z}[k] \in \mathbb{R}$ be the time-domain measurement the sensor obtained at time step k, then we can define measurement vector $\hat{\mathbf{z}}$ can be defined as:

$$\hat{\mathbf{z}} = \hat{z}\left[\forall k \in \mathcal{K}\right] = \left(\hat{z}[1], \ldots, \hat{z}[n_k]\right)^\top \in \mathbb{R}^{n_k} \ . \tag{2.1}$$

Without loss of generality, we model sensor imperfections $\boldsymbol{\zeta}$ as the sum of a constant sensor bias $\delta \in \mathbb{R}$ and random measurement error vector $\boldsymbol{\nu} = (\nu[1], \ldots, \nu[n_k])^\top \in \mathbb{R}^{n_k}$. Hence, the full signal model can be represented as shown in Equation (2.2).

$$\hat{\mathbf{z}} = \mathbf{z} + \boldsymbol{\zeta} = \mathbf{z} + \boldsymbol{\nu} + \delta \ . \tag{2.2}$$

Given these definitions, we can define the signal energy with which the occupant localization is derived. In this study, we employ the energy of the measured vibro-measurement vector as the localization feature. The formal definition of the localization feature is given in Definition 2.4.

Definition 2.4 (Energy of Vibro-measurement Vector)**.** Energy of a random measurement vector can be obtained by employing Rayleigh's Energy Theorem, given in Proposition A.1, on the random vibro-measurement vectors $\hat{\mathbf{z}}$. The energy of a vibro-measurement vector is formally given below,

$$\hat{e} = \|\hat{\mathbf{z}}\|_2^2 = \hat{\mathbf{z}}^\top \hat{\mathbf{z}} = \sum_{k=1}^{n_k} \hat{z}[k]^2 \ . \tag{2.3}$$

Because we model vibro-measurements as random vectors, the energy representation of the measurement vector is also random as shown below.

$$\hat{e} = e + \varepsilon \ , \tag{2.4}$$

where $e = \|\mathbf{z}\|_2^2$ and ε represent the energy of the true signal and error in energy representation.

By using the definition of the energy of vibro-measurement vectors, we can now formally define a localization function that determines the occupant location $\hat{\mathbf{x}}$ from the energy e of the measurement vector $\mathbf{z}$.

Definition 2.5 (Energy-based Vibro-localization Function $\mathbf{h}(e;\cdot)$)**.** Without loss of generality, we provide an abstract definition of a localization function that maps the energy of an vibro-measurement vector to a location vector. The equation below represent this localization function in terms of the distance d and the directionality θ defined between the sensor and the occupant. In other words, when the true energy e is known, the localization function $\mathbf{h}(e;\cdot)$ should yield the true location $\mathbf{x}$.

$$\mathbf{x} = \mathbf{h}(e;\cdot) = d \begin{bmatrix} \cos\theta \\ \\ \sin\theta \end{bmatrix} . \tag{2.5}$$

By using the same representation, we can derive the estimated location vector $\hat{\mathbf{x}}$ from the energy $\hat{e}$ of a noisy and bias drifted vibro-measurement $\hat{\mathbf{z}}$ vector as shown below,

$$\hat{\mathbf{x}} = \mathbf{h}(\hat{e};\cdot) = \hat{d} \begin{bmatrix} \cos\hat{\theta} \\ \\ \sin\hat{\theta} \end{bmatrix} . \tag{2.6}$$

Given the definition of the estimated and true location vectors, i.e., $\hat{\mathbf{x}}$ and $\mathbf{x}$, we can now define a vector representing the localization error. A successful vibro-localization technique should minimize all statistical moments of this error vector when repeated measurements are done.

Definition 2.6 (Localization Error)**.** The localization error $\boldsymbol{\chi} \in \mathbb{R}^2$ can be defined

as:

$$\boldsymbol{\chi} = \mathbf{x} - \hat{\mathbf{x}} \ . \tag{2.7}$$

Hence, the magnitude of the estimation error can then be represented as the norm of the difference between the estimated and the true location as,

$$\|\boldsymbol{\chi}\| = \|\mathbf{x} - \hat{\mathbf{x}}\| \ . \tag{2.8}$$

Figure 2.1 provides a graphical representation of the defined terminology.

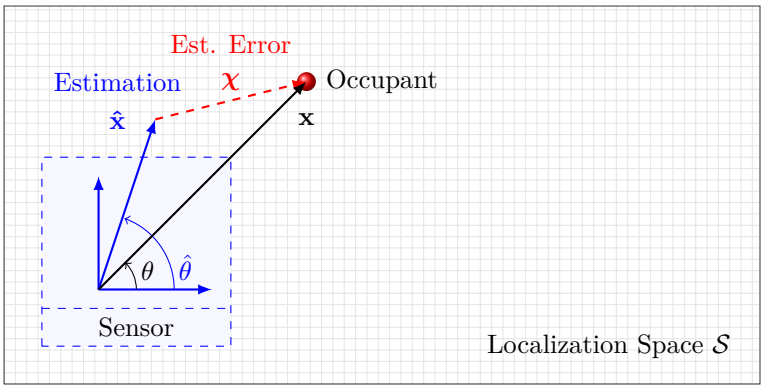

Figure 2.1: This figure graphically demonstrates the terminology defined in this chapter. As can be seen in the figure, the localization function $\mathbf{h}(\hat{e}; \cdot)$ provides an estimated location vector $\hat{\mathbf{x}}$ when the true occupant location is $\mathbf{x}$.

Definition 2.7 (Accuracy and Precision)**.** The statistical properties of localization error $\boldsymbol{\chi}$ define the *accuracy* and *precision* of a vibro-localization system. Accuracy is a measure of how close the estimated localizations are to the true values, typically represented by the mean of the error vector, $\boldsymbol{\mu}_{\boldsymbol{\chi}}$. A smaller mean error indicates higher accuracy, as it implies that on average, the estimations are closer to the true location. Precision, on the other hand, refers to the consistency of the estimations,

often quantified by the covariance matrix $\boldsymbol{\Sigma}_{\boldsymbol{\chi}}$. The covariance provides a measure of the spread of the localization errors around the mean. A smaller covariance implies higher precision, indicating that the estimations are more consistently clustered around the mean, regardless of whether that mean is close to the true value. Thus, $\boldsymbol{\mu}_{\boldsymbol{\chi}}$ and $\boldsymbol{\Sigma}_{\boldsymbol{\chi}}$ are directly related to the accuracy and precision of the localization system, respectively.

2.3 Method

In this chapter, we delve into the methodological aspects of quantifying and analyzing the errors inherent in single-sensor energy-based vibro-localization. Our approach is grounded in a rigorous statistical framework, aimed at comprehensively understanding and mitigating the uncertainties that impact vibro-localization accuracy. We focus on the energy of the vibro-measurement vector and its error characteristics, recognizing that these form the crux of the localization process. Through this methodology, we aim to strengthen the reliability and precision of vibro-localization techniques in practical applications.

In this work, we operate under a set of assumptions to streamline our analysis. Firstly, we consider the error in directionality to be negligible, with the difference $|\theta - \hat{\theta}|$ approximating zero. Regarding the measurement errors, we model the random measurement error $\nu[k]$ as independent and identically distributed (iid) realizations of a normally distributed random variable $\nu \sim \mathcal{N}\left(0, \sigma_{\zeta}^2\right)$ with zero mean and standard deviation $\sigma_{\zeta} \in \mathbb{R}^{+}$. Additionally, we ensure that the number of samples n_k is

sufficiently large, specifically $n_k \geq 20$, to ensure reliable statistical analysis. For the sake of brevity, we assume in this chapter that the energy e of the true signal $\mathbf{z}$ is known.

Lemma 2.1. *If random measurement error* $\nu[k] \sim \mathcal{N}\left(0, \sigma_\zeta^2\right)$ *and* iid*, then signal energy is* approximately *normally distributed.*

Proof. In light of the assumptions above, the error in the calculated energy can be stated as,

$$\varepsilon = \hat{e} - e = \sum_{k=1}^{n} \hat{z}[k]^2 - \sum_{k=1}^{n} z[k]^2 \tag{2.9a}$$

$$= \sum_{k=1}^{n} \hat{z}[k]^2 - z[k]^2 = \sum_{k=1}^{n} \left(z[k] + \nu[k] + \delta\right)^2 - z[k]^2 \sim \mathcal{N}\left(\mu_\varepsilon, \sigma_\varepsilon^2\right) \tag{2.9b}$$

where $\mu_\varepsilon = n\left(\delta^2 + \sigma_\nu^2\right) + 2\delta \sum z[k]$, $\sigma_\varepsilon = 2n\sigma_\nu^2\left(2\delta^2 + \sigma_\nu^2 + 2e\right)$ and $\mathcal{N}\left(\mu, \sigma^2\right)$ denotes the PDF of the Normal distribution with the mean μ and standard deviation σ. Therefore, the density of the error in the signal energy can be derived as shown below,

$$\boxed{\varepsilon \sim f_\varepsilon\left(\varepsilon\right) = \mathcal{N}\left(\mu_\varepsilon, \sigma_\varepsilon^2\right) = \frac{1}{\sigma_\varepsilon\sqrt{2\pi}} \exp\left(-\frac{1}{2}\left(\frac{\varepsilon - \mu_\varepsilon}{\sigma_\varepsilon}\right)^2\right).} \tag{2.10}$$

In light of this derivation, the expected error in the calculated energy is a function of the number of samples in the signal n, bias δ and the standard deviation of the random errors σ_ζ. □

A pivotal aspect of our methodology involves the Parametric Energy Decay Model, a

crucial tool in understanding the dynamics of energy decay in vibro-localization. This model encapsulates the relationship between the energy of vibro-measurements and the corresponding spatial parameters. Specifically, it characterizes how the energy of a vibro-measurement vector decays with respect to distance, thereby providing a fundamental link between the measurable energy and the occupant's location. The model is defined mathematically as follows:

Definition 2.8 (Parametric Energy Decay Model)**.** The Parametric Energy Decay Model is an analytical tool used to describe the relationship between the energy of vibro-measurement vectors and the distance to the source of the vibration. This model is crucial for understanding how energy dissipates over space, which directly impacts the localization accuracy in vibro-localization systems. The model is defined with two key parameters, β and e^*, where β (a negative real number) represents the rate of energy decay and e^* (a positive real number) signifies a reference energy level. The distance d to the vibration source is a function of the measured energy e, given by:

$$d = g(e; \beta, e^*) = \frac{1}{\beta} \log \frac{e}{e^*} \ . \tag{2.11}$$

Similarly, the estimated distance $\hat{d}$ is derived from the estimated energy $\hat{e}$, following the same functional form:

$$\hat{d} = g(\hat{e}; \beta, e^*) = \frac{1}{\beta} \log \frac{\hat{e}}{e^*} \ . \tag{2.12}$$

The role of θ, the direction angle of the occupant relative to the accelerometer, is also critical in the context of localizing the source. By applying these formulations to the

established localization function (Equation (2.5)), we can quantify the magnitude of the localization error in terms of energy measurement errors. This is represented as the norm of the vector $\boldsymbol{\chi}$, which quantifies the difference between the estimated and actual location:

$$\boxed{\|\boldsymbol{\chi}\| = \Delta_{\varepsilon}\left(\varepsilon;\beta\right) = -\frac{1}{\beta}\log\left(\frac{\hat{e}}{e}\right) = -\frac{1}{\beta}\log\left(\frac{e+\varepsilon}{e}\right) = -\frac{1}{\beta}\log\left(1+\frac{\varepsilon}{e}\right).} \tag{2.13}$$

2.3.1 PDF of the Localization Error

PDF transformation theorem allows us to derive the PDF of a function of random variable when the function is invertible. Formal definition of this theorem is given in Proposition A.4.

By employing normed localization error $\|\boldsymbol{\chi}\|$ from the PDF of the calculated energy errors, we have:

$$f_{\|\boldsymbol{\chi}\|}\left(\|\boldsymbol{\chi}\|\right) = f_{\varepsilon}\left(\Delta_{\varepsilon}^{-1}(\|\boldsymbol{\chi}\|)\right)\left|\frac{\partial}{\partial\|\boldsymbol{\chi}\|}\Delta_{\varepsilon}^{-1}\left(\|\boldsymbol{\chi}\|\right)\right| \tag{2.14a}$$

$$= -\beta e\exp\left(\beta\|\boldsymbol{\chi}\|\right)f_{\varepsilon}\left(e\exp\left(\beta\|\boldsymbol{\chi}\|\right)-e\right) \tag{2.14b}$$

where $\Delta_{\varepsilon}^{-1}(\|\boldsymbol{\chi}\|) = e\exp\left(\beta\|\boldsymbol{\chi}\|\right) - e$ and $|\frac{\partial}{\partial\|\boldsymbol{\chi}\|}\Delta_{\varepsilon}^{-1}\left(\cdot\right)| = -\beta e\exp\left(-\beta\|\boldsymbol{\chi}\|\right)$. Finally

putting everything together, we derive PDF of localization error:

$$\boxed{\Rightarrow f_{\|\boldsymbol{\chi}\|}\left(\|\boldsymbol{\chi}\|\right) = -\frac{\beta e \exp\left(\beta \|\boldsymbol{\chi}\|\right)}{\sigma_\varepsilon \sqrt{2\pi}} \exp\left(-\frac{\left(e \exp\left(\beta \|\boldsymbol{\chi}\|\right) - e - \mu_\varepsilon\right)^2}{2\sigma_\varepsilon^2}\right) .} \tag{2.15}$$

Remark 2.1. Equation (2.15) implies that $f_{\|\boldsymbol{\chi}\|}\left(\|\boldsymbol{\chi}\|\right)$ follows a normal distribution iff the error function Δ_ε is linear.

With the calculated PDF derived in Equation (2.15), we can derive the mean and the variance of the normed error term as:

$$\boxed{\mu_{\|\boldsymbol{\chi}\|} = \mathbb{E}\left[\|\boldsymbol{\chi}\|\right] = \int_0^\infty \|\boldsymbol{\chi}\| \; f_{\|\boldsymbol{\chi}\|}\left(\|\boldsymbol{\chi}\|\right) \, \mathrm{d}\, \|\boldsymbol{\chi}\|} \tag{2.16}$$

and

$$\boxed{\sigma^2_{\|\boldsymbol{\chi}\|} = \mathrm{Var}\left[\|\boldsymbol{\chi}\|\right] = \mathbb{E}\left[\|\boldsymbol{\chi}\|^2\right] = \int_0^\infty \|\boldsymbol{\chi}\|^2 \; f_{\|\boldsymbol{\chi}\|}\left(\|\boldsymbol{\chi}\|\right) \, \mathrm{d}\, \|\boldsymbol{\chi}\|} \tag{2.17}$$

As can be seen in the equations above, the closed form solution for the mean and variance is computationally challenging due to the complexity of the integrals involved. In order to tackle this problem, we employ an numerical method that enables us to calculate the moments of the normed localization error from the PDF of the energy error $f_\varepsilon\left(\varepsilon\right)$ and error function $\Delta_\varepsilon(\varepsilon)$.

2.3.2 First Statistical Moment of Localization Error

In order to derive the first moment, i.e., the mean, of the localization error, LOTUS is employed. LOTUS is a theorem used to calculate the expectation of a function of random variable with its own PDF. Hence, we can state the mean as given by,

$$\mu_{\|\boldsymbol{\chi}\|} = \mathbb{E}\left[\Delta_{\varepsilon}(\varepsilon)\right] = \int \Delta_{\varepsilon}(\varepsilon)\, f_{\varepsilon}\left(\varepsilon\right)\, \mathrm{d}\varepsilon \ . \tag{2.18}$$

Furthermore, we employ Taylor expansion to the error function $\Delta_{\varepsilon}(\varepsilon)$ around $\frac{\mu_{\varepsilon}}{e}$ to analytically obtain the value of the integral given in Equation (2.18).

$$\Delta_{\varepsilon}(\varepsilon) \approx \hat{\Delta}_{\varepsilon}(\varepsilon) = \frac{1}{\beta}\left(-\log\left(\frac{\mu_{\varepsilon}}{e}+1\right) + \sum_{k=1}^{\infty} \frac{(-1)^{k}}{k\left(e+\mu_{\varepsilon}\right)^{k}}\left(\varepsilon-\mu_{\varepsilon}\right)^{k}\right) \tag{2.19}$$

This analytical approach is as given by,

$$\mu_{\|\boldsymbol{\chi}\|} \approx \hat{\mu}_{\|\boldsymbol{\chi}\|} = \int \hat{\Delta}_{\varepsilon}(\varepsilon)\, f(\varepsilon)\, d\varepsilon \ ,$$

where $\hat{\Delta}_{\varepsilon}(\varepsilon)$ is approximated using its Taylor series expansion around μ_{ε}. Expanding the error function $\hat{\Delta}_{\varepsilon}(\varepsilon)$, we obtain,

$$\approx \int -\frac{1}{\beta}\left(\log\left(\frac{\mu_{\varepsilon}}{e}+1\right) - \sum_{k=1}^{\infty} \frac{(-1)^{k}}{k\left(1+\mu_{\varepsilon}\right)^{k}}\left(\varepsilon-\mu_{\varepsilon}\right)^{k}\right)\, f(\varepsilon)\, d\varepsilon \ .$$

Further we split the integral into two parts: one involving the 0^{th} approximation and the other involving the higher orders,

$$= -\frac{1}{\beta}\int \log\left(\frac{\mu_\varepsilon}{e}+1\right) f(\varepsilon)\, d\varepsilon + \frac{1}{\beta}\int \sum_{k=1}^{\infty} \frac{(-1)^k}{k\,(e+\mu_\varepsilon)^k}\,(\varepsilon-\mu_\varepsilon)^k\; f(\varepsilon)\, d\varepsilon\ .$$

The first integral evaluates to the logarithmic term times the integral of the probability density function over all space, and the second integral is expanded term-by-term,

$$= -\frac{1}{\beta}\log\left(\frac{\mu_\varepsilon}{e}+1\right)\int f(\varepsilon)\, d\varepsilon + \frac{1}{\beta}\sum_{k=1}^{\infty}\int \frac{(-1)^k}{k\,(e+\mu_\varepsilon)^k}\,(\varepsilon-\mu_\varepsilon)^k\; f(\varepsilon)\, d\varepsilon\ .$$

Each term in the series is integrated separately, and these integrals correspond to the central moments of the distribution of ε.

$$= -\frac{1}{\beta}\log\left(\frac{\mu_\varepsilon}{e}+1\right) + \frac{1}{\beta}\sum_{k=1}^{\infty}\int \frac{(-1)^k}{k\,(e+\mu_\varepsilon)^k}\,(\varepsilon-\mu_\varepsilon)^k\; f(\varepsilon)\, d\varepsilon$$

The series is expressed in terms of the central moments, denoted as α_k.

$$= -\frac{1}{\beta}\log\left(\frac{\mu_\varepsilon}{e}+1\right) + \frac{1}{\beta}\sum_{k=1}^{\infty}\frac{(-1)^k}{k\,(e+\mu_\varepsilon)^k}\int (\varepsilon-\mu_\varepsilon)^k\; f(\varepsilon)\, d\varepsilon$$

Finally, using the definition of α_k for even and odd terms, the expression is simplified to its final form.

$$= -\frac{1}{\beta}\log\left(\frac{\mu_\varepsilon}{e}+1\right) + \frac{1}{\beta}\sum_{k=1}^{\infty}\frac{(-1)^k\,\alpha_k}{k\,(e+\mu_\varepsilon)^k}\ ,$$

where $\alpha_{2k} = (2k-1)!!\sigma_\varepsilon^{2k}$ and $\alpha_{2k+1} = 0$; therefore,

$$\boxed{\mu_{\|\boldsymbol{\chi}\|} \approx \hat{\mu}_{\|\boldsymbol{\chi}\|} = -\frac{1}{\beta}\log\left(\frac{\mu_\varepsilon}{e}+1\right) + \frac{1}{2\beta}\sum_{k=1}^{\infty}\frac{(-1)^{2k}\,(2k-1)!!\sigma_\varepsilon^{2k}}{k\,(e+\mu_\varepsilon)^{2k}\,e^{2k}}\ .} \tag{2.20}$$

Remark 2.2. As can be seen in Equation (2.20), the mean vibro-localization error is zero, iff $\mu_\varepsilon = \sigma_\varepsilon = 0$.

2.4 Parametric Study and Results

This section presents a parametric study of the single-sensor energy-based vibro-localization technique. The study focuses on the impact of sensor noise and Signal-to-noise Ratio (SNR) on the localization accuracy. The methodological approach combines theoretical and empirical analyses, primarily using a Taylor series approximation and numerical integration.

The localization error was analytically estimated by expanding the error function $\Delta_\varepsilon(\varepsilon)$ using a Taylor series. This approach allowed for an approximate calculation of the mean localization error across different orders of approximation. The study varied key parameters like the SNR and the standard deviation of the sensor noise σ_ε to observe their effects on the localization accuracy.

The results, illustrated in Figure 2.2, show the percent error in mean localization estimation across different SNR values (-5 dB, 0 dB, and 5 dB) and varying σ_ε (1, 3, and 5). The Taylor series approximation was considered up to the 4th order. The

findings indicate that:

- Higher SNR values generally result in lower percent errors, highlighting the significance of SNR in vibro-localization accuracy.
- Increasing σ_ε leads to higher percent errors, demonstrating the sensitivity of the localization process to sensor noise.
- The accuracy of the Taylor series approximation improves with higher orders, as evidenced by the decrease in percent error.

The parametric study underscores the importance of considering sensor noise characteristics and SNR in designing and deploying vibro-localization systems. The Taylor series approximation provides a useful tool for estimating the mean localization error, especially in scenarios where exact analytical solutions are challenging to derive. Even with smaller approximation order ($k \leq 5$), the proposed numeracial approach was able to identify the localization error.

2.5 Conclusions

This chapter explored the uncertainties in single-sensor energy-based vibro-localization techniques. The study revealed:

- Both sensor noise and SNR significantly affect the accuracy of vibro-localization. Higher SNR and lower sensor noise improve localization precision.

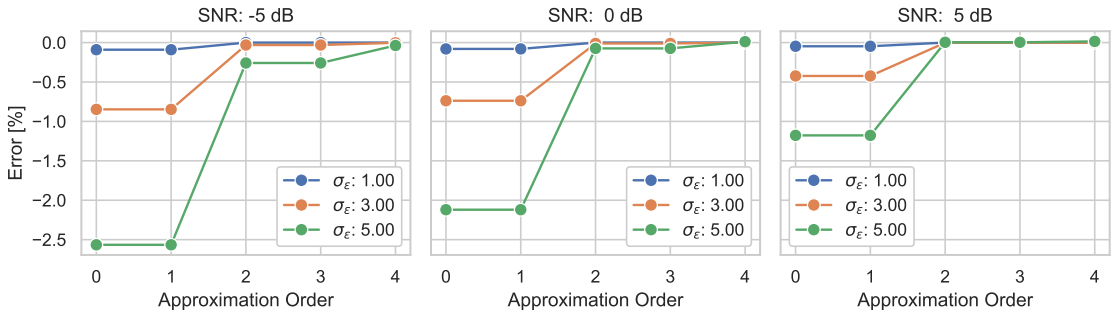

Figure 2.2: This figure illustrates the percent error in the mean localization estimation across varying signal-to-noise ratio (SNR) levels of -5 dB, 0 dB, and 5 dB, and different standard deviations of sensor noise σ_ε values of 1, 3, and 5. The analysis is conducted using a Taylor series approximation up to the 4th order. The results depict the sensitivity of vibro-localization accuracy to both SNR and sensor noise, highlighting the reduction in percent error with increasing SNR and decreasing sensor noise. The improvement in approximation accuracy with higher-order Taylor series expansions is also evident.

- The use of a Taylor series approximation for the mean localization error is effective, especially for higher-order expansions.
- Localization errors seldom follow a normal distribution.
- The mean localization error is never zero if the vibro-measurement vectors contain inherent errors.

The following chapter explores the multi-sensor setups in which a sensor fusion technique was employed to combine the localization results of each sensor to compensate for the limitations identified in single-sensor systems with empirical studies.

Chapter 3

Energy-based Vibro-Localization Technique with Multiple Sensors

3.1 Introduction

In this chapter, we consider a multi-sensor energy-based vibro-localization technique to localize an occupant in an indoor environment. This localization technique can be considered as extension of the single-sensor vibro-localization technique presented in the earlier chapter. As shown in the earlier chapter, the mean localization error $\mu_{\|\boldsymbol{\chi}\|}$ is a function of both mean μ_ε and standard deviation σ_ε of the energy estimations. We, furthermore, showed the mean localization error $\mu_{\|\boldsymbol{\chi}\|}$ can minimized by minimizing μ_ε and σ_ε.

The dynamics of accelerometers are known to be affected by many internal and external factors in their employment such as changes in temperature, humidity, etc. In our framework, these changes manifest themselves in the mean μ_ε and standard deviation σ_ε of energy error estimates. Hence, they are are seldom zero. In other words, even calibrated sensors are not ideal.

In light of the observations so far, it is imperative for a vibro-localization system to employ multiple sensors at the same time to capture multiple observations of the same phenomenon, i.e., the footstep, in attempt to reduce the localization errors. This chapter describes the a multi-sensor vibro-localization technique that has employs a multi-objective loss function in the localization framework to minimize two types of localization errors: (i) internal errors accounting for measurement errors and (ii) external errors accounting for floor dispersion and other propagation-related errors.

The methods, experiments, and other relevant information presented in this chapter has already been through the peer-review process and resulted in the journal paper [8].

3.1.1 Baseline Study and Overview of the Fundamental Differences

In this subsection, we present a comprehensive comparison between the established baseline in vibro-localization, as outlined by Alajlouni and Tarazaga [1], and the proposed technique [8]. The fundamental differences between these two methodologies are summarized in Table 3.1. The comparison encompasses the key elements of vibro-localization, including the type of localization features measured, the known parameters assumed in both techniques, the calibrated parameters used during offline processing, and the final output produced during online processing. This comparative analysis aims to highlight the enhancements and novel contributions of the proposed technique.

	Baseline Technique [1]	**Proposed Technique**
Localization Feature (Measured)	Energy Measurements $e_1, \ldots, e_m$	Energy Measurements $e_1, \ldots, e_m$
Known Parameters (*A priori*)	Sensor locations $\mathbf{t}_1, \ldots, \mathbf{t}_m$	Sensor locations $\mathbf{t}_1, \ldots, \mathbf{t}_m$
Calibrated Parameters (Offline Processing)	None	Sensor noise profile: μ_ζ, σ_ζ Calibration vectors $\boldsymbol{\beta}_1, \ldots, \boldsymbol{\beta}_m$
Output (Online Processing)	Location estimate: $\hat{\mathbf{x}}$	Location estimate: $\mathbf{x}^*$ Consensus set: $\mathcal{C}$ and its distribution: $f_{\mathcal{C}}(\mathbf{x})$

Table 3.1: Comparative Overview of Baseline and Proposed Vibro-localization Techniques. This table illustrates the key differences in localization features, known and calibrated parameters, and output between the Baseline Technique as per Alajlouni and Tarazaga [1] and the proposed technique [8].

In contrast, our study builds upon and extends this model by considering non-linear factors that may affect the energy-distance relationship. These factors could include environmental characteristics and multi-path effects, which cannot be accounted for in a purely linear model.

To emphasize the contributions of this study, it is essential to contrast our approach with the closest related work, as encapsulated in [3]. While [3] initiates the exploration of the problem space by deriving PDFs of the energy of acquired vibro-measurement vectors, it does so with the simplifying assumption of neglecting the cross-terms as they are zero mean random variables. Our work diverges fundamentally at this juncture, where we incorporate all terms in our derivation. This inclusion introduces a more comprehensive model that acknowledges the potential influence of cross-terms.

Further diverging from [3], we abandon the assumption that energy measurements e_i

are independent and identically distributed. This work demonstrates, through Proof 1 and Corollary 1, that the e_i's are, in fact, sampled from distinct distributions for each sensor. We substantiate this claim by providing the PDFs and the first two statistical moments for these distributions. This nuanced understanding of the energy measurements' distribution is pivotal to enhancing the accuracy of vibro-localization techniques, thereby marking a significant stride forward from the state-of-the-art.

3.1.2 Summary of the Contributions

This paper presents an energy-based vibro-localization technique that addresses the sensor imperfections and their effects on the localization results. The proposed technique employs a family of accelerometers placed on a floor to generate multiple vibro-measurement vectors about the same step. Furthermore, the proposed technique employs two corrective steps in the localization time: (i) a comprehensive uncertainty quantification to minimize the effect of the internal errors occurring during the signal acquisition time present in the vibro-measurement vectors; and, (ii) an information-theoretic BSE algorithm to address the external sources of uncertainty such as reflections and dispersion. The following points summarize the proposed technique's contributions.

- **Vibro-localization Technique with Comprehensive Uncertainty Quantification** (Addressing Limitations 1 and 2): The proposed vibro-localization technique employs an explicit error model for each sensor. Therefore, a complete uncertainty quantification on the localization errors due to the measure-

ment errors can be minimized with our technique.

- **Information-Theoretic BSE Algorithm** (Addressing Limitation 3): The paper introduces a BSE algorithm. The proposed BSE algorithm divides the sensors into two distinct subsets: the ones that show some consistency amongst them, and the ones which are divergent in nature. By leveraging a greedy information-theoretic approach, it decides whether a sensor should be placed in the former set, or vice versa. This algorithm guarantees a locally-optimal subset of the sensors in minimizing the localization errors.

- **Empirical Validation** (Addressing Limitations 1–3): Data from a previously conducted controlled experiments were employed to validate and benchmark the proposed technique. The results demonstrated significant improvements over the baseline [1] approach in terms of both accuracy and precision.

- **Quantification of the Empirical Precision and Accuracy** (Addressing Limitation 3): This paper employs the results of the empirical validation study to quantify an empirical correlation between precision and accuracy achieved with the proposed vibro-localization technique. By employing such correlation metrics, we gain better insights about the technique's performance and failures.

3.1.3 Outline

This chapter focuses on the uncertainties in multi-sensor energy-based vibro-localization techniques. The structure of the chapter is as follows:

1. Section 3.1 introduces the context and significance of employing multiple sensors in vibro-localization, building upon the single-sensor technique explored in the previous chapter. This section lays the groundwork for understanding the need for multi-sensor setups to improve localization accuracy and mitigate uncertainties.

2. Section 3.2 defines the multi-sensor localization problem, including the mathematical formulation of sensor measurements and the representation of localization space. This section also introduces the concept of energy-based vibro-localization for multiple sensors and establishes the necessary theoretical foundations.

3. Section 3.3 elaborates on the methodology for quantifying and analyzing errors in multi-sensor vibro-localization. It discusses the parametric energy decay model for multiple sensors, the formulation of joint probability density functions (PDFs), and the sensor fusion technique. The section also introduces the Byzantine Sensor Elimination (BSE) algorithm, which is crucial for filtering out misleading sensor data.

4. Section 3.4 details the experimental setup used to validate and benchmark the proposed multi-sensor vibro-localization technique. This includes the description of the test environment, sensor configuration, data collection process, and the specific steps involved in implementing the proposed method.

5. Section 3.5 presents the results and findings from the experimental validation. It includes statistical analysis of localization errors, comparisons with baseline

techniques, and insights into the performance of the proposed method under various scenarios and sensor configurations.

6. Section 3.6 summarizes the key findings of the chapter, discusses the implications of the proposed multi-sensor vibro-localization technique, and suggests potential directions for future research in the field of vibro-localization.

This outline provides a structured overview of the chapter, guiding the reader through the development and evaluation of the multi-sensor energy-based vibro-localization technique.

3.2 Problem Definition

In this study we consider a localization problem where m number of sensors are employed in the occupant localization. Let $\mathcal{M} \triangleq \{1, \ldots, m\}$ be the index set of all the sensors and sensor $i \in \mathcal{M}$ be located at $\mathbf{t}_i$ in a rectangular localization space $\mathcal{S}$. Consider a localization problem where i^{th} sensor's measurements are employed to estimate location vector $\mathbf{x}_i \in \mathcal{R}^2$ when the occupant is actually located at $\mathbf{x} \in \mathcal{R}^2$. This sensor layout is illustrated in as depicted in Figure 3.1.

Definition 3.1 (Measurement of Sensor i)**.** Let $\hat{z}_i[k] \in \mathbb{R}$ be the time-domain measurement the sensor obtained at time step k, then we can a define measurement vector $\hat{\mathbf{z}}_i$ concerning the measurements of sensor i during the time steps $k \in \mathcal{K} = \{1, \ldots, n_k\}$

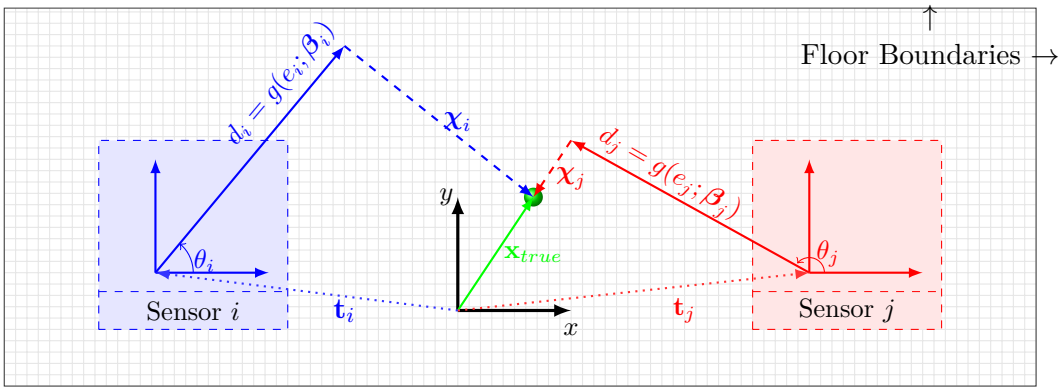

Figure 3.1: This figure visualizes some key variables frequently used in the paper. The blue and red box represent sensor i and sensor j which reside at $\mathbf{t}_i$ and $\mathbf{t}_j$, respectively. When an occupant excites the floor with their footstep which is occured at $\mathbf{x}_{true}$, m accelerometers first estimate $\forall d_i \in \{1, \ldots, m\}$. Therefore, the estimated location vector of the occupant location by sensor i can be seen as the vector summation of its location vector $\mathbf{t}_i$ and the estimated d_i for some θ_i.

can be defined as:

$$\hat{\mathbf{z}}_i = \hat{z}_i \left[\forall k \in \mathcal{K}\right] = \left(\hat{z}_i[1], \ldots, \hat{z}_i[n_k]\right)^\top \in \mathbb{R}^{n_k} \text{ and } \forall\, i \in \mathcal{M}. \tag{3.1}$$

Following the similar definitions, we model imperfections of sensor i^{th} $\boldsymbol{\zeta}_i$ as the sum of a constant sensor bias $\delta_i \in \mathbb{R}$ and random measurement error vector $\boldsymbol{\nu}_i = (\nu_i[1], \ldots, \nu_i[n_k])^\top \in \mathbb{R}^{n_k}$. Hence, the full signal model can be represented as shown in Equation (3.2).

$$\hat{\mathbf{z}}_i = \mathbf{z}_i + \boldsymbol{\zeta}_i = \mathbf{z}_i + \boldsymbol{\nu}_i + \delta_i \ . \tag{3.2}$$

Definition 3.2 (Measured Signal Energy e_i and Error in Signal Energy ε_i)**.** We follow the same definition presented in Definition 2.4. The added subscript in the

notation of measured energy, $\hat{e}_i$, true energy e_i, and error in the energy, ε_i, denote to which sensor these variables correspond. This relationship is formally stated as,

$$\hat{e}_i = e_i + \varepsilon_i, \ \forall\, i \in \mathcal{M} \ . \tag{3.3}$$

By using the definition of the energy of vibro-measurement vectors, we can now formally define a localization function that determines the occupant location $\hat{\mathbf{x}}_i$ from the energy e_i of the measurement vector $\mathbf{z}_i$.

Definition 3.3 (Energy-based Vibro-localization Function $\mathbf{h}(e;\cdot)$)**.** We follow the same definition presented in Definition 2.5. Please notice the added subscript i to the defined variables.

We provide an abstract definition of a localization function that maps the energy of an vibro-measurement vector to a location vector. The equation below represent this localization function in terms of the distance $d_i = \|\mathbf{x} - \mathbf{t}_i\|$ and the directionality θ_i defined between the sensor i and the occupant.

In other words, when the true energy e is known, the localization function $\mathbf{h}(e_i;\cdot)$ should yield the true location $\mathbf{x}$.

$$\mathbf{x}_i = \mathbf{h}(e_i;\cdot) = \mathbf{t}_i + d_i \begin{bmatrix} \cos\theta_i \\ \\ \sin\theta_i \end{bmatrix} \ . \tag{3.4}$$

By using the same representation, we can derive the estimated location vector $\hat{\mathbf{x}}$ from

the energy $\hat{e}$ of a noisy and bias drifted vibro-measurement $\hat{\mathbf{z}}$ vector as shown below,

$$\hat{\mathbf{x}}_i = \mathbf{h}(\hat{e}_i; \cdot) = \mathbf{t}_i + \hat{d} \begin{bmatrix} \cos\hat{\theta}_i \\ \\ \sin\hat{\theta}_i \end{bmatrix} . \tag{3.5}$$

Given the definition of the estimated and true location vectors, i.e., $\hat{\mathbf{x}}_i$ and $\mathbf{x}$, we can now define a vector representing the localization error. A successful vibro-localization technique should minimize all statistical moments of this error vector when repeated measurements are done.

Definition 3.4 (Localization Error)**.** The localization error $\boldsymbol{\chi}_i \in \mathbb{R}^2$ can be defined as:

$$\boldsymbol{\chi}_i = \mathbf{x} - \hat{\mathbf{x}}_i \ . \tag{3.6}$$

3.3 Method

In this work, we operate under a set of assumptions to streamline our analysis. Firstly, we consider the directionality θ_i is modeled as a random variable that is distributed uniformly between $[0, 2 * \pi)$, implying complete lack of knowledge about it. Regarding the measurement errors, we model the random measurement error $\nu[k]$ as independent and identically distributed (iid) realizations of a normally distributed random variable $\nu \sim \mathcal{N}\left(0, \sigma_\zeta^2\right)$ with zero mean and standard deviation $\sigma_\zeta \in \mathbb{R}^+$. Additionally, we ensure that the number of samples n_k is sufficiently large, specifically

$n_k \geq 20$, to ensure reliable statistical analysis.

In this work, the parametric energy decay model $g_i(\cdot)$ is assumed to be a monotonically decreasing function for some positive energy measurement $e_i \in \mathbb{R}_+$; therefore, it is bijective and its inverse exists.

By employing the PDF transformation theorem to obtain the PDF of the estimated location vector $\hat{\mathbf{x}}_i$ as shown in Equation (3.7).

$$\Rightarrow f_{\mathbf{X}_i}\left(\mathbf{x}_i; e_{true,i}, \boldsymbol{\beta}_i\right) = \frac{\left|\frac{\partial g_i^{-1}}{\partial \mathbf{x}_i}\left(\|\mathbf{x}_i - \mathbf{t}_i\|; \boldsymbol{\beta}_i\right)\right|}{\|\mathbf{x}_i - \mathbf{t}_i\|\,\sigma_E (2\pi)^{\frac{3}{2}}} \exp\left[-\frac{\left(g_i^{-1}\left(\|\mathbf{x}_i - \mathbf{t}_i\|\right) - \mu_E\right)^2}{2\sigma_E^2}\right] \tag{3.7}$$

Equation (3.7) shows the PDFs $f_{\mathbf{X}_i}(\cdot)$ assign a probability value for an occupant located at vector $\mathbf{x}_i$ given the inverse of the parametric decay function $g(\cdot)$ and sensor location $\mathbf{t}_i$. Notice the term in the denominator, i.e., $\|\mathbf{x}_i - \mathbf{t}_i\|$, in Equation (3.7) resulting in an inverse relationship between the probability values and the distance between the sensor and the impact location.

3.3.1 Sensor Fusion

Given the PDFs $f_{\mathbf{X}_i}\left(\mathbf{x}_i; e_{true,i}, \boldsymbol{\beta}_i\right)$ for all sensors indexed by $i \in \mathcal{M}$, we aim to find a joint-PDF that represents the collective localization outcome using the vibro-measurements of m sensors. As all the sensors are independent of each other, we can represent the joint-PDF as given below:

$$f_{\mathbf{X}_1,\ldots,\mathbf{X}_m}\left(\mathbf{x}_1,\ldots,\mathbf{x}_m; e_{true,1},\ldots,e_{true,m},\boldsymbol{\beta}_1,\ldots,\boldsymbol{\beta}_m\right) = \prod_{i=1}^{m} f_{\mathbf{X}_i}\left(\mathbf{x}_i; e_{true,i},\boldsymbol{\beta}_i\right) \ . \quad (3.8)$$

Let $\kappa_i = \dfrac{e_{true,i}}{e_i}$ be an independent variable denoting the ratio between the unknown true energy $e_{true,i}$ and measured signal energy e_i. Notice that $e_i = e_{true,i} + \epsilon_i$; thus, $\kappa_i = 1 + \Delta$ for small Δ. Given this definition, we can reparameterize the joint-PDF which forms the basis for the sensor fusion algorithm used in this paper,

$$f_{\mathbf{X}_1,\ldots,\mathbf{X}_m}\left(\mathbf{x}_1,\ldots,\mathbf{x}_m; \kappa_1,\ldots,\kappa_m,\boldsymbol{\beta}_1,\ldots,\boldsymbol{\beta}_m\right) = \prod_{i=1}^{m} f_{\mathbf{X}_i}\left(\mathbf{x}_i; \kappa_i,\boldsymbol{\beta}_i\right) \ . \quad (3.9)$$

3.3.2 Byzantine Sensor Elimination

Byzantine sensors, as illustrated in Figure 3.2, are those that provide misleading or incorrect data, often deviating from the true value or introducing conflicting information into a sensor network. In the figure, sensors A and B are examples of informative sensors (shown in image (a) and (b)) while C and D are instances of Byzantine sensors (image (c) and (d)). The PDFs of the Byzantine sensors have a sharp peak indicating high precision, but they show offsets from the true value, revealing their low accuracy. When such a sensor's data is fused with data from other sensors, it can significantly distort the resulting joint likelihood, leading to erroneous conclusions or alternative hypotheses about the occupant's location.

The second row of the figure provides insights into the effects of fusing data from a

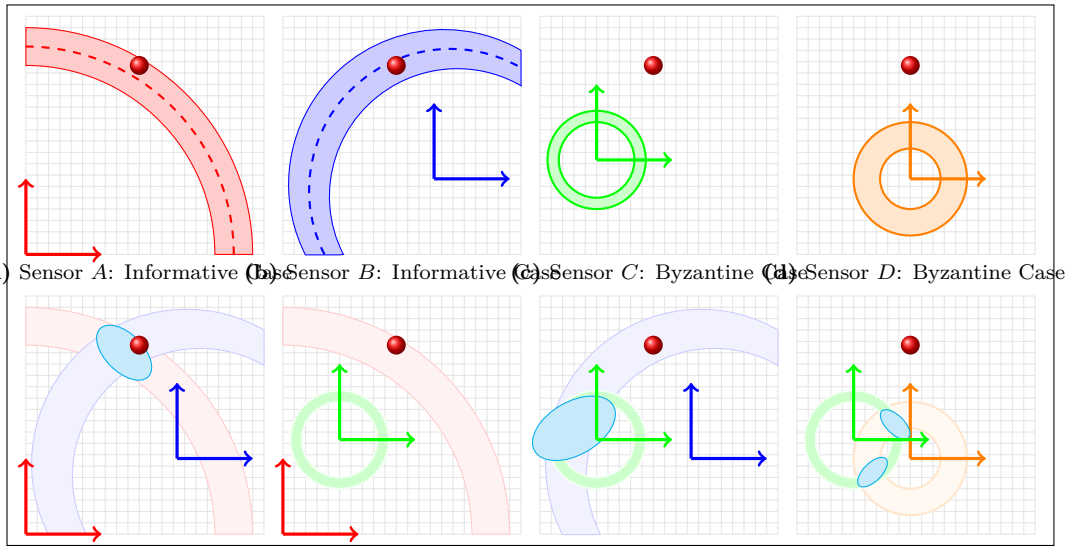

(a) Sensor A: Informative Case **(b)** Sensor B: Informative Case **(c)** Sensor C: Byzantine Case **(d)** Sensor D: Byzantine Case

(e) Sensor A + Sensor B **(f)** Sensor A + Sensor C **(g)** Sensor B + Sensor C **(h)** Sensor C + Sensor D

Figure 3.2: The figure displays eight labeled images (a) to (h) in two rows. The first row depicts individual sensor PDFs: (a) Sensor A with a sharp peak for high precision, (b) Sensor B with a broader curve for accuracy and lower precision, (c) Sensor C, a Byzantine sensor with an offset sharp peak, and (d) Sensor D with a flat curve indicating low accuracy and precision. The second row illustrates fusion results: (e) a unimodal curve from sensors A and B showing enhanced precision, (f) a uniform distribution from sensors A and C indicating discord, (g) an offset peak from sensors B and C suggesting an alternative location hypothesis, and (h) a bimodal distribution from sensors C and D with peaks deviating from the true value. The figure highlights the challenges of fusing data from diverse sensors, especially with Byzantine influences.

Byzantine sensor with informative ones. For instance, image (f) showcases the fusion result of an informative Sensor A with the Byzantine Sensor C. The resulting uniform distribution across the localization space highlights the lack of consensus between the two, emphasizing the detrimental impact of the Byzantine sensor on the fusion process. Similarly, image (g) depicts the fusion of Sensor B with Sensor C, producing an offset peak that suggests an alternative hypothesis about the occupant's location.

To ensure the reliability of a sensor network, it's crucial to identify and eliminate such Byzantine influences. By observing the fusion results and identifying distributions that deviate from expected patterns or the true value, one can iteratively pinpoint and remove Byzantine sensors, enhancing the overall accuracy and trustworthiness of the network.

In a vibro-localization systems, there exist many factors that can easily render a sensor as Byzantine. For instance, the parametric energy decay model assumes the wavefronts detected by an accelerometer travel the direct path from the step location to the sensor observing the vibration phenomenon. However, this assumption seldom holds for indoor environment as the wavefronts may be reflected by various objects or boundaries that exists in the environment. To address and circumvent these undesired scenarios, we introduce an algorithm that identifies a consensus-forming subset of sensors within $\mathcal{M}$ to counteract the influence of Byzantine sensors.

During the initialization phase of the information-theoretic BSE algorithm, a comprehensive computation is carried out to determine all conceivable pairwise joint-PDFs and their corresponding entropies. Subsequently, an initial consensus set is established using the sensor pair (i, j) that produces the maximum entropy after fusion from a distinct pair of the index set $\mathcal{M}$. Formally, this set is expressed as:

$$\mathcal{C} = \left\{ i, j \mid \underset{i,j}{\operatorname{argmax}} \, \mathbb{E}\left[-\log f_{\mathbf{x}_i, \mathbf{x}_j}(\mathbf{x}) \right] \right\} . \tag{3.10}$$

The joint-PDF encapsulating the existing consensus at any point in time, denoted

as $f_{\mathcal{C}}(\mathbf{x})$, is derived as follows:

$$f_{\mathcal{C}}(\mathbf{x}) \triangleq \prod_{\forall i \in \mathcal{C}} f_{\mathbf{X}_i}(\mathbf{x}; \kappa_i, \boldsymbol{\beta}_i) \tag{3.11}$$

Throughout each iterative phase, a candidate sensor, denoted as k (which is distinct from the pair (i, j)), is selected from the set $\mathcal{M}$. This sensor undergoes an evaluation against the prevailing consensus set $\mathcal{C}$, achieved by fusing its PDF with the consensus PDF $f_{\mathcal{C}}(\mathbf{x})$. A subsequent determination is predicated upon the entropy, or more precisely, the surprisal of the resulting hypothesis in with respect to the current consensus. Should the integration of sensor k not attenuate the joint-PDF to a uniform distribution (as exemplified in case (f) in Figure 3.2) or not decrease the average entropy, it is incorporated into the consensus set. Otherwise, sensor k is classified as Byzantine. Finally, the above procedure undergoes an iterative repetition with varying vectors of $\boldsymbol{\kappa} = (\kappa_1, \ldots, \kappa_m)^\top$. This iteration progresses in the direction of the gradient of the $f_{\mathcal{C}}(\mathbf{x})$ calculated with respect to $\boldsymbol{\kappa}$ vector. The process persists until a local maxima in the entropy landscape, corresponding to a (possibly locally-)optimal consensus, is identified. The proposed BSE algorithm, coupled with the vibro-localization technique, is outlined in Algorithm 3.1.

In the initialization phase of the proposed algorithm, the consensus set $\mathcal{C}$ is constructed by selecting the pair of sensors (i, j) whose fused PDF exhibits the maximum entropy $h_{i,j}$. This approach is deliberately chosen to preserve a diverse set of hypotheses regarding the target location. By maximizing the entropy at this stage, the algorithm ensures that it does not prematurely discard potential valid hypothe-

Algorithm 3.1 Vibro-localization using the Information-Theoretic BSE Algorithm

procedure BSE($f, \mathcal{M}, \mathcal{S}$)
  $h^* \leftarrow -\infty$
  for all $(i, j) \in \mathcal{M} \times \mathcal{M}$, $i \neq j$ **do** ▷ Initialization of the consensus set
    $h_{i,j} \leftarrow \textsc{entropy}(\textsc{fuse}(f_{\mathbf{x}_i}, f_{\mathbf{x}_j}), \mathcal{S})$
    if $h_{i,j} \geq h^*$ **then**
      $h^*, \mathcal{C} \leftarrow h_{i,j}, \{i, j\}$
    end if
  end for
  for all $i \in \mathcal{M} \setminus \mathcal{C}$ **do** ▷ Attempt to expand the consensus set
    $h_i \leftarrow \textsc{entropy}(\textsc{fuse}(f_{\mathcal{C}}, f_{\mathbf{x}_i}), \mathcal{S})$
    if $h_i \leq h^*$ **then**
      $h^*, \mathcal{C} \leftarrow h_i, \mathcal{C} \cup \{i\}$
    end if
  end for
  return $\mathcal{C}$
end procedure
$\boldsymbol{\kappa} \leftarrow \mathbf{1}_{m \times 1}$
while $\|\nabla \boldsymbol{\kappa}\| \leq thr$ **do** ▷ Gradient Descent
  $\boldsymbol{\kappa} += \nabla \boldsymbol{\kappa}$ ▷ Update $\boldsymbol{\kappa}$ in the gradient direction
  $f_{\mathbf{x}_1}, \ldots, f_{\mathbf{x}_m} \leftarrow \textsc{density-projection}(e_1, \ldots, e_m, \boldsymbol{\kappa})$
  $\mathcal{C} \leftarrow \text{BSE}(f_{\mathbf{x}_1}, \ldots, f_{\mathbf{x}_m}, \mathcal{M}, \mathcal{S})$
  $f_{\mathcal{C}} \leftarrow \text{FUSE}(f_{\mathbf{x}_i} \ \forall i \in \mathcal{C})$
  $\mathbf{x}^* = \text{argmax}_{\mathbf{x} \in \mathcal{S}} f_{\mathcal{C}}(\mathbf{x})$
end while

ses that could be crucial for accurate localization. This is particularly important in environments where the presence of Byzantine sensors—sensors that may provide misleading or false information—is a concern. Maximizing entropy mitigates the risk of the initial consensus being overly influenced by such sensors, as they might produce similar deceptive densities that could dominate the consensus if entropy were minimized.

Subsequently, the algorithm attempts to expand the consensus set by incorporating

additional sensors $k \in \mathcal{M} \setminus \mathcal{C}$ that contribute meaningful information. A sensor is included in the consensus set only if its fusion with the current consensus PDF $f_{\mathcal{C}}(\mathbf{x})$ results in a decrease in entropy, i.e., $h_i \leq h^*$. This criterion ensures that any new sensor added to the consensus set provides information that refines and enhances the existing hypothesis about the target location without introducing significant uncertainty. By progressively incorporating sensors that reduce entropy, the algorithm balances the need to maintain a comprehensive set of hypotheses while incrementally improving the precision of the localization. This iterative process continues until a local maximum in the entropy landscape is reached, corresponding to an optimal or near-optimal consensus that effectively mitigates the influence of Byzantine sensors.

At an initial glance, readers might find similarities between the algorithm above and the RANSAC algorithm [27], an acronym for Random Sample Consensus; however, they are fundamentally distinct. RANSAC is an algorithm employed in fields such as computer vision and computational geometry to robustly estimate model parameters, even in the presence of outliers. In contrast, the information-theoretic BSE algorithm is tailored for sensor networks to counteract Byzantine sensors using information-theoretic strategies. While both algorithms seek to establish reliability (or robustness) and consensus (or agreement) within datasets, their approaches, and primary use cases are notably distinct. A side-by-side comparison of their characteristics is presented in Table 3.2.

	RANSAC	Mirshekari et al. [45]	Information-theoretic BSE
Primary Use	Estimating parameters of mathematical models in the presence of outliers, predominantly in computer vision.	Elimination of far-away sensors in an adaptive multilateration technique of a vibro-localization system.	Elimination of Byzantine sensors in sensor networks of vibro-localization systems by using information theory.
Methodology	Works by randomly selecting subsets of data and identifying the model with the highest consensus.	Identifying distant sensors in TDoA estimations to avoid bias in multilateration algorithm.	Derives a consensus among sensors based on entropies of likelihoods to emphasizes robustness against malicious sensors.
Input Type	Points	Time-domain measurements	PDFs

Table 3.2: Comparison between RANSAC, [45], and Information-theoretic BSE algorithm

3.4 Experiments

The proposed technique's effectiveness and performance were assessed through a series of controlled experiments, the details of which are outlined in this section.

3.4.1 Experimental Setup

To evaluate our vibro-localization approach, we employed the empirical data from a set of controlled experiments in a corridor situated on the 4^{th} floor of Goodwin Hall, an operational building on Virginia Tech's campus. In these experiments, two participants traversed a pre-defined 16-meter path. Figure 3.3 represents the step locations

constituting the traversed path—represented with green circles (○)—as well as the sensor locations—represented with black squares (■)—overlayed. We derived our reference points from these investigations and utilized identical experimental data as in [1] and [3]. The corridor's concrete floor housed the sensors, which were attached to uniform steel mounts welded to the flanges of the structural I-beams beneath. In this study, the experimental testbed utilized is embedded within the structural framework of the building. Due to this integration, a photograph of the testbed would not substantially add to the understanding of the setup, as it predominantly features standard structural components of the building. The crucial aspects of our setup are its configuration and the placement of sensors and equipment, which are more effectively conveyed through the schematic representation provided in Figure 3.3. Eleven PCB Piezotronics model 352B accelerometers, detecting dynamic out-of-plane acceleration within the frequency range of (2, 10000) Hz and with an average sensitivity of 1000 millivolts per g (where $g = 9.8m/s^2$), recorded the structural vibrations. These devices captured data from 162 steps taken by each participant, amounting to a total of 324 steps. The data collection was facilitated by VTI Instruments EMX-4250 digital signal analyzer cards, connected to the accelerometers via coaxial cables and equipped with anti-aliasing filters and a high-precision 24-bit Analog-to-Digital-Converter. The accelerometer data was sampled at a rate of 1024 Hz. For a comprehensive insight into the experimental design, readers are directed to the foundational study [1].

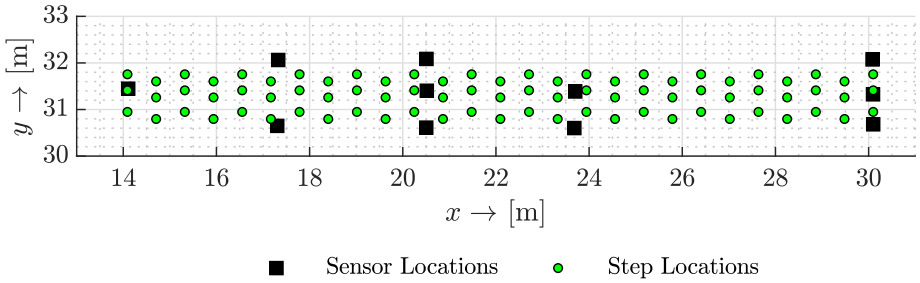

Figure 3.3: This figure demonstrates the test-bed used in the controlled experiments. The green circles represent the unique step locations while the black squares mark the sensor locations used in the experiments.

Data and Model Validity: The preliminary study gathered vibration data during low-activity periods, ensuring minimal movement in the vicinity of the instrumented corridor. The data revealed that the sensors' noise profiles were normally distributed with zero mean and consistent variance. Thus, the signal model in Equation (3.2) aptly represents the vibration measurements. Given this observation, we confidently state that the energy-related random variables, represented as e_i for $i \in \mathcal{M}$, align with the experimental findings.

Signal Detection Problem: A primary distinction exists between our implementation of the baseline and the original work presented in their publication [1]: the signal detection algorithm. The baseline study, in its methodology, adopted a tight-window approach. This approach was characterized by the identification of the first time instance that the signal breaks the SNR envelope and the peak of the signal. In this study, on the other hand, we used a stochastic signal detection algorithm denote the time steps which the signal magnitude breaks the noise floor and eventually dissipates below the noise floor. To contrast our method, the detection algorithm

employed in this study took a more flexible stance: instead of strictly searching for the time instance we signal peaks, our algorithm was designed to be more lenient. It permitted "silent" periods, which are intervals without significant signal activity, both before and after the vibration. This choice of algorithm led to a notable difference in the signal energy values when compared to the baseline study. Figure 3.4 graphically demonstrates the difference between the signal detection algorithm employed by the baseline and the proposed technique with an impulse response curve of an underdamped second-order system. The black line represents the elements of the "noisy" vibro-measurement vector. The dashed red and green lines represent the results of the baseline and proposed detection algorithm, respectively. This distinction in approach not only highlights the variability in signal processing techniques but also underscores the potential impact of these choices on the final results and interpretations.

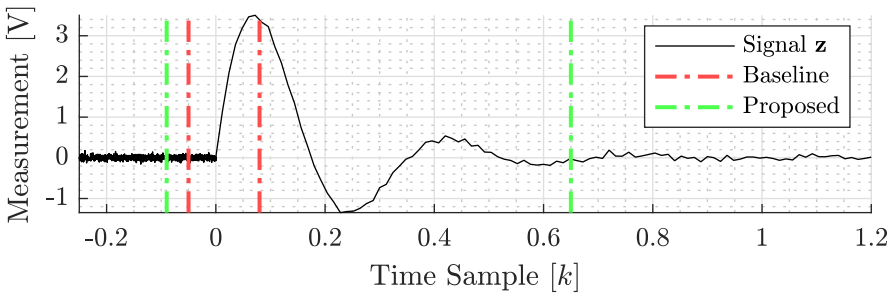

Figure 3.4: This figure demonstrates the differences between signal (step) detection algorithms employed by the baseline and proposed techniques. The black line (—) represents the noisy measurements of a second-order system. The green dashed line (— -) represents the proposed "relaxed" detection results employed in this study. On the other hand, the red dashed line (— -) represents the signal detection algorithm employed by the baseline study.

3.4.2 Implementation

In the course of our data processing, we discretized the localization space $\mathcal{S}$. This discretization was achieved by segmenting it into a total of 270,000 grid cells, specifically arranged in a 300×900 configuration. By evaluating the PDFs only at the center of each grid cell, we avoided the intricate surface integrals and achieved greater computational efficiency.

The calibration vectors $\boldsymbol{\beta}_i$ are obtained in an offline processing step, where the signal energy and their known distance measurements are used to fit the parametric decay models denoted as $g_i(e_i)$. These measurements can be easily obtained by exciting the floor, for instance, by hitting it with a hammer, at known locations within the localization space. This process facilitates the accurate calibration of the system by correlating the known physical impacts at specific points with the resulting signal characteristics. In this work, we only used the first 27 steps of a Occupant-1's data to obtain these calibration vectors for all sensors.

In the online processing, when a footstep detection is made, the signal energy of the vibration measurements are used to minimize the log-transformed loss function Equation (3.11) by adjusting the value of vector $\boldsymbol{\kappa} = (\kappa_1, \ldots, \kappa_m)^\top$ in the direction of its gradient. Consequently, information-theoretic BSE algorithm was employed each iteration of gradient descent to discard Byzantine sensors. The steps of gradient descent is repeated until the algorithm converges a solution and forms a consensus among the sensor

To evaluate the proposed technique, we employed a combinatorial study to analyze

the effect of the number of sensors used on the localization metrics. Specifically, we employed all the possible combinations of $m = \{2, \ldots, 11\}$ with the given sensor configuration in the experimental data. This yields $n_{cases} = \sum_{i=2}^{11} \binom{11}{i} = 2036.00$ number of cases to evaluate for each step and occupant. In other words, each step is reevaluated 2036.00 times, yielding 329,832.00 (2036.00 $\times$ 162) data points for each occupant. Therefore, in our analysis, we are able to provide different defining statistical characteristics of the localization error. This approach also enables us to remedy various uncertainty sources such as the effects of sensor placement, and differences in propagation paths while enriching the results independent of the individual sensor performance.

3.5 Results

This section presents the empirical outcomes derived from our proposed vibro-localization technique. These empirical results benchmark the efficacy of our approach in terms of accuracy, and precision. By analyzing these findings in detail, we aim to provide a deeper look into the technique's performance under various conditions and scenarios.

In Figure 3.5, three representative sets (out of 659,664.00 cases) of outcomes are depicted, each corresponding to a different number of sensors ($m = 2, 6, 11$) employed for the localization of identical step data for two occupants. The left column presents results for the first occupant, while the right column pertains to the second occupant. Sensor locations within this figure are marked by square markers (■), and sensors deemed non-Byzantine by the algorithm are highlighted with circular markers (○).

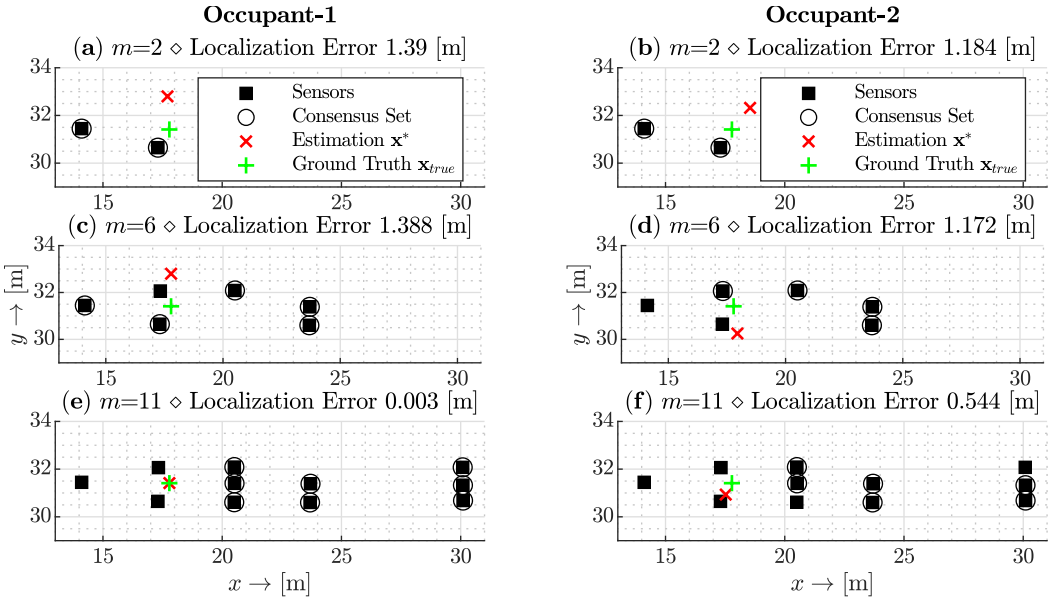

(a) An illustrative result of the 1^{st} occupant's data.

(b) An illustrative result of the 2^{nd} occupant's data.

Figure 3.5: Localization outcomes for two distinct occupants using varying sensor counts ($m = 2, 6, 11$). The left column represents the first occupant's result set and the right, the second occupant's result set. Square markers indicate sensor locations, circles denote non-Byzantine sensors, while green pluses and red crosses symbolize the ground truth and estimated locations, respectively. Errors for configurations (a) to (e) show progressive refinement with increased sensors, highlighting the algorithm's adaptability and precision.

The green plus (+) and red cross (×) markers respectively represent the ground truth $\mathbf{x}_{\text{true}}$ and the estimated location vector $\mathbf{x}^*$. In the scenarios labeled (a) for the first occupant and (b) for the second, utilizing two sensors, the norm of localization errors are 1.39 and 1.18 meters, respectively. Both sensors are considered as the consensus set due to the lack of alternative sensor choices. As the sensor count increases to six, as shown in labels (c) for the first occupant and (d) for the second, the observed errors were 1.39 for the first occupant and 1.17 meters for the second occupant.

However, the first occupant's results do not show significant improvement with the additional sensors. In these cases, the initial sensors were adaptively substituted with new sensors for consensus. With a further increase to eleven sensors, as indicated in labels (e) and (f), the localization errors reduce to 0.30 centimeters for the first occupant and 54.40 centimeters for the second, both accompanied by an updated consensus set.

To evaluate the influence of sensor count on localization outcomes, especially in terms of accuracy and precision, the quantile function, represented as $x = Q(p)$, of the localization error was plotted against the number of sensors, as illustrated in Figures 3.6 and 3.7. This function yields the error value x for a given probability p, satisfying the condition $\mathrm{P}(X \leq x) = p$. In essence, it serves as the inverse of the CDF for the random variable x. For clarity, $Q(0.5)$ corresponds to the median of the localization error across varying sensor counts.

In Figure 3.6, the quartiles of sample localization errors—the first (25^{th} percentile), second (50^{th} percentile or median), and third (75^{th} percentile)—are plotted against the number of sensors available in the localization system. In other words, the number of sensors listed in the figure represents the sensor count before the proposed BSE algorithm eliminates a subset from the sensor pool. The data for the first and second occupants are differentiated by red and black colors, respectively. For the first occupant, the solid (–), dashed (– -), and dotted (· ·) red lines represent the respective quartiles of the localization error. For the second occupant, the solid (–), dashed (– -), and dotted (· ·) black lines serve the same purpose. The figure indicates a reduction in localization error with an increasing number of sensors. This trend is

consistent across all quartiles. Notably, as more sensors are introduced, the disparity between the first and third quartiles diminishes, highlighting enhanced accuracy in both optimal and suboptimal conditions.

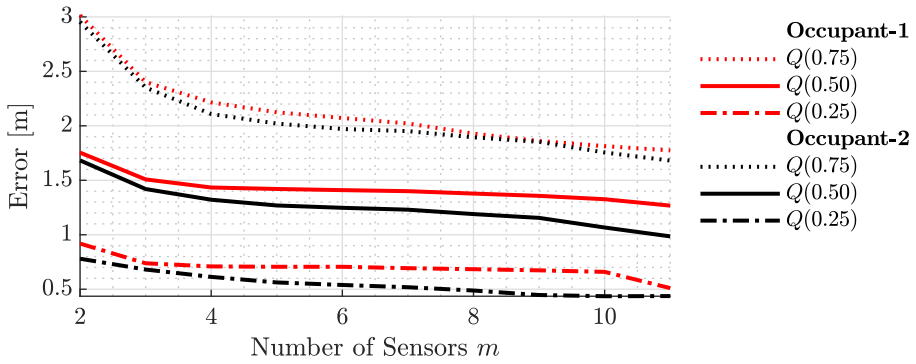

Figure 3.6: Quartile analysis of sample localization errors against the number of sensors before the proposed BSE algorithm was employed. The plot showcases a consistent reduction in errors across all quartiles with an increasing number of sensors, highlighting improved consistency in both best- and worst-case scenarios.

As it is evident in Table 3.5, a consistent trend across both occupants and all quartiles were seen: as the number of sensors increases, the localization error (measured in all metrics) decreases. For instance, the median error for the first occupant decreases from 2.45 with two sensors to 1.79 meters with eleven sensors in the proposed technique (see Table 3.5). Similarly, for the second occupant, it reduces from 2.39 to 1.61 meters for the same number of sensors. The standard deviation, representing the error variability, also shows a steady decrease, an evidence of a growth in consistency, as more sensors are employed. This reduction in error and variability is a clear indication of enhanced accuracy and reliability in the localization process.

Figure 3.7 presents the precision of the entire localization system in terms of entropy, or the surprisal, encoded in the joint-PDFs. Akin to the previous figure, the data

for the first and second occupants are differentiated by red and black colors, and the same styling is used to represent the same quartiles. The figure distinctly shows a decrease in uncertainty as the number of sensors grows. This trend is consistent across all quartiles. Significantly, with the addition of more sensors, the gap between the first and third quartiles narrows, indicating enhanced precision in both best- and worst-case scenarios.

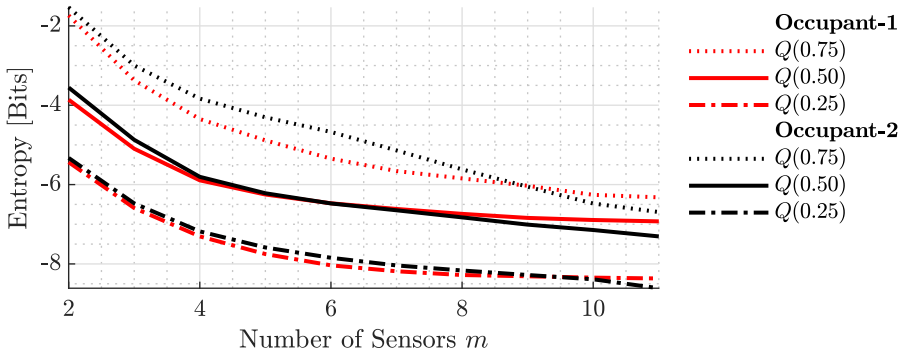

Figure 3.7: Entropy-based precision of the localization system for varying sensor counts. Red and black lines differentiate data for the first and second occupants. The figure underscores reduced uncertainty with more sensors, highlighting enhanced precision across all quartiles.

Figure 3.8 synthesizes the insights derived from Figure 3.6 and Figure 3.7, demonstrating a discernible correlation between accuracy and precision metrics obtained with the proposed localization technique. The figure demonstrates that enhancements in precision are parallel with improvements in accuracy. This trend can be observed for both of the occupants even with different numbers of sensors used in the localization system. This trend, as can be seen in the figure, can be described as quasi-linear curves where the range of the lines differs with the number of sensors used in the technique. Also, it can be seen in the figure that sub-meter localization

accuracy is viable even with two sensors if the sensors yield a certain level of measurement precision. On the other hand, for the higher number of sensors, this goal is more attainable as their curves span more in the sub-meter region. Furthermore, note that the magnitude of the improvement in accuracy with the improved precision differs for different numbers of sensors employed in the system. In other words, more desirable results become prominent when more sensors are used.

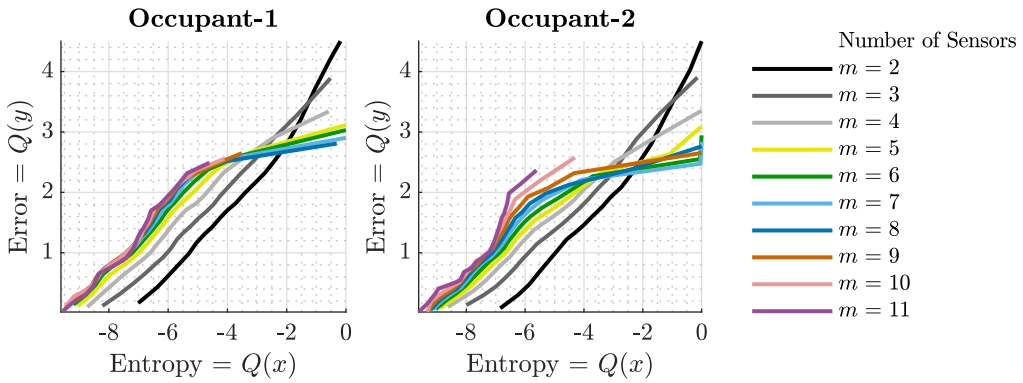

Figure 3.8: This figure shows a Quantile-Quantile plot between the precision and accuracy metrics observed in the experimental data. The figure provides evidence for the correlation between precision and accuracy for varying numbers of sensors.

The empirical-PDFs and empirical-CDFs are non-parametric tools employed to analyze the distribution of data points in a sample without assuming an inherent distribution. The empirical-PDFs provide a histogram-like representation, highlighting the relative frequencies of various data values, while the empirical-CDFs capture the cumulative probability for each value. Figure 3.9 depicts the empirical-PDF, represented with solid lines, and CDF, represented with dashed lines, of the normed localization error derived from location estimates for both occupants' data. The plots on the left and right represent these curves of the first and second occupants' data,

respectively. The solid blue and brown curves represent the empirical-PDF of the proposed and baseline techniques while the dashed curves represent the empirical-CDF. As can be seen in the figures the proposed technique shows relatively higher accumulations in lower regions in the error axis than the baseline suggesting the error characteristics of the proposed technique will more likely fall on the smaller regions than the baseline. Another way to present this observation is through the empirical-CDFs. For instance, a major takeaway from the empirical-CDF curves is that 80% of the errors of the proposed and baseline techniques are equal or less than 2.29 and 3.10 meters for both occupants, respectively.

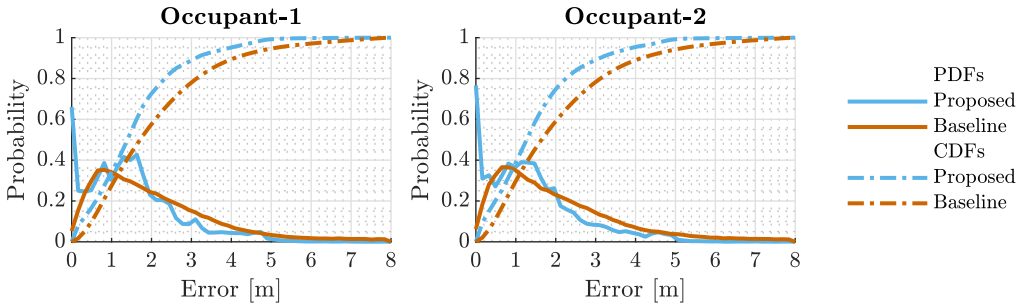

Figure 3.9: Empirical-PDFs and CDFs of normed localization errors derived from location estimates for both occupants. Solid lines represent the empirical-PDFs, with blue and brown indicating the proposed and baseline techniques, respectively. Dashed lines depict the empirical-CDFs. The plots demonstrate that the proposed technique generally results in lower localization errors compared to the baseline.

Table 3.5 tabulates the overall landscape of resulting error characteristics of the proposed technique and the baseline by providing a statistical analysis comparing the performance of two localization methods. Various descriptive statistical metrics such as mean, standard deviation, median, root mean square (RMS), minimum, and maximum values, all expressed in meters, are presented. The results span varying

numbers of sensors, from 2 to 11, and are differentiated for two distinct occupants.

For the first occupant, the proposed method consistently outperforms the baseline across all metrics. The weighted average mean localization error for the proposed method is 1.58 meters, a notable improvement from the baseline's 2.31 meters. Similarly, for the second occupant, the proposed method achieves a weighted average mean error of 1.48 meters, significantly lower than the baseline's 2.28 meters. Also, one interesting finding from this result set is that the proposed localization technique can achieve sub-meter localization accuracy and precision when enough sensors are employed (cf. Std. Dev. of Occupant-1 and 2 with 10 and 11 sensors; cf. median localization error of Occupant-2 with 11 sensors). This table underlines the enhanced accuracy and precision of the proposed vibro-localization technique over the baseline for various sensor configurations and both occupants.

In Figures 3.10 and 3.11, we analyze the relationship between average sensor distance and localization error for two scenarios: considering all sensors and after BSE algorithm is applied. We used regression analysis to understand error behavior, with the slope indicating error increase as occupants move farther from sensors. Correlation between error and sensor distance assesses technique effectiveness in removing systemic errors from the localization technique. Ideal localization technique should minimize these slope and correlation. Table 3.3 compares our results with [45].

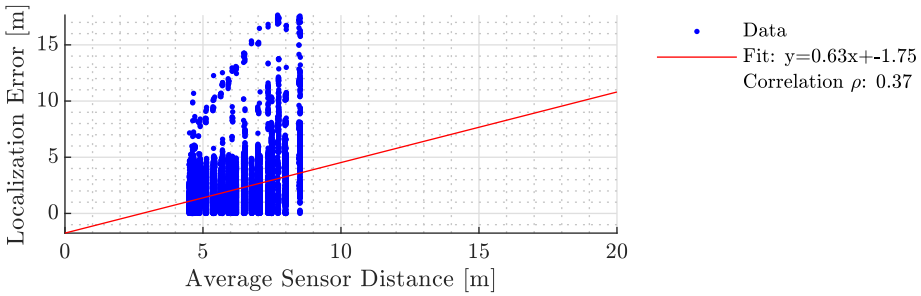

Figure 3.10: The error characteristics of the proposed method as a function of average sensor distance when all sensors were considered.

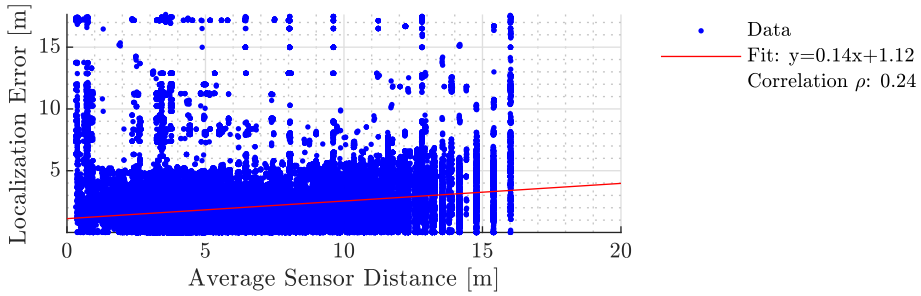

Figure 3.11: The error characteristics of the proposed method as a function of average sensor distance when a subset of the sensors were considered.

3.6 Conclusions

In this study, we proposed a novel vibro-localization technique that can address two types of uncertainty sources: (i) uncertainties due to sensor imperfections, and (ii) uncertainties due to complexities of wave propagation. To achieve minimum localization errors, the proposed technique coupled with an information-theoretic BSE algorithm employs an uncertainty quantification on the error contributions of to the sensors. By doing so, the proposed technique minimizes the effect of the errors present in the vibro-measurement technique as well as other sources of uncertainties mentioned above.

	Work presented in [45]		Proposed	
	Without SE	With SE	Without SE	With SE
Slope	1.44	0.56	**0.63**	**0.14**
Intercept	**-2.3**	**-0.56**	1.75	1.12
Correlation Coefficient	0.82	**0.24**	**0.37**	**0.24**

Table 3.3: A systemic comparison between the results of work presented in [45] and the proposed localization technique. SE stands for Sensor Elimination.

In order to benchmark the proposed method, we employed a set of previously-conducted controlled experiments. The essence of this validation study was to gauge the efficacy and performance of our proposed technique, especially when contrasted against an existing methodology in the literature. In the experimental setup, which consisted of two participants traversing a 16-meter path, the structural vibrations captured by the closest eleven accelerometers among a much bigger family of accelerometers available in the environment are used. The proposed technique provided significant improvements in almost all localization metrics while best-case and worst-case scenarios became less extreme. The proposed localization technique coupled with the proposed BSE algorithm yielded a 31.47% decrease in mean localization error.

In this study, we established a consistent empirical relationship between two key metrics of localization systems: accuracy and precision. A localization system's accuracy may not be known post-deployment, we can always determine its precision from the estimates it provides. Therefore, the empirical relationship between these two metrics may be employed to estimate the system's accuracy without recalibrating it. Although the link between accuracy and precision might be inferential, it has important consequences for the use of these systems in practice.

Table 3.4: Comparison of baseline and proposed methods for different numbers of sensors and cases for two occupants. The table presents statistical measures such as mean, standard deviation, median, root mean square (RMS), minimum, and maximum values in meters. Baseline algorithm is adapted from [1].

		Mean [m]		**Std. Dev.** [m]		**Median** [m]		**RMS** [m]		**Min** [m]		**Max** [m]	
# Sensors	# Cases	[1]	Proposed	[1]	Proposed	[1]	Proposed	[1]	Proposed	[1]	Proposed	[1]	Proposed
2	55	3.69	2.32	3.34	2.33	2.45	1.75	4.97	3.28	0.01	0.00	16.02	7.57
3	165	2.90	1.85	2.60	1.77	1.96	1.51	3.90	2.56	0.01	0.00	16.01	7.57
4	330	2.51	1.65	2.14	1.41	1.92	1.43	3.30	2.17	0.01	0.00	14.91	7.48
5	462	2.29	1.56	1.81	1.20	1.80	1.42	2.92	1.97	0.00	0.00	14.14	7.48
6	462	2.15	1.52	1.57	1.11	1.79	1.41	2.66	1.88	0.00	0.00	13.23	1.88
7	330	2.05	1.49	1.40	1.07	1.78	1.40	2.49	1.83	0.01	0.00	12.44	1.88
8	165	1.99	1.45	1.28	1.04	1.76	1.38	2.36	1.79	0.01	0.00	11.79	8.33
9	55	1.93	1.41	1.19	1.02	1.76	1.36	2.27	1.74	0.02	0.00	10.60	5.03
10	11	1.89	1.37	1.12	1.00	1.74	1.33	2.20	1.70	0.02	0.00	9.33	4.90
11	1	1.85	1.31	1.08	0.98	1.79	1.27	2.14	1.63	0.18	0.00	7.46	4.64
Weighted Average		2.31	1.58	1.79	1.25	1.84	1.43	2.92	2.02	0.01	0.00	13.67	14.16

Table 3.5: Comparison of baseline and proposed methods for different numbers of sensors and cases for two occupants. The table presents statistical measures such as mean, standard deviation, median, root mean square (RMS), minimum, and maximum values in meters. Baseline algorithm is adapted from [1].

		Mean [m]		**Std. Dev.** [m]		**Median** [m]		**RMS** [m]		**Min** [m]		**Max** [m]	
# Sensors	# Cases	[1]	Proposed	[1]	Proposed	[1]	Proposed	[1]	Proposed	[1]	Proposed	[1]	Proposed
2	55	3.71	2.17	3.37	2.10	2.39	1.68	5.01	3.02	0.02	0.00	16.03	17.66
3	165	2.91	1.80	2.65	1.71	1.96	1.42	3.93	2.48	0.00	0.00	16.01	16.93
4	330	2.50	1.58	2.18	1.42	1.85	1.32	3.32	2.12	0.01	0.00	14.07	16.73
5	462	2.27	1.46	1.85	1.23	1.77	1.27	2.92	1.91	0.01	0.00	13.02	16.73
6	462	2.11	1.41	1.61	1.13	1.71	1.25	2.65	1.80	0.00	0.00	12.32	16.73
7	330	2.01	1.37	1.43	1.09	1.70	1.23	2.47	1.75	0.01	0.00	11.36	9.03
8	165	1.93	1.33	1.31	1.06	1.65	1.19	2.33	1.70	0.01	0.00	10.87	5.81
9	55	1.87	1.29	1.22	1.02	1.65	1.15	2.24	1.64	0.01	0.00	8.72	5.07
10	11	1.83	1.24	1.16	0.97	1.67	1.07	2.16	1.57	0.03	0.00	6.95	4.97
11	1	1.79	1.17	1.12	0.92	1.61	0.99	2.11	1.49	0.11	0.00	5.90	3.89
Weighted Average		2.28	1.48	1.82	1.25	1.78	1.28	2.92	1.94	0.01	0.00	12.76	14.25

We have used this correlation to devise a method for estimating the system's accuracy during operation without the need for additional calibration. Notably, this correlation holds true across different users, which suggests that our findings are robust and widely applicable. Additionally, our results offer a standardized approach to designing experiments. With the established correlation, the number of sensors required for an experiment can be decided based on the desired accuracy and the sensor precision.

Delving deeper into the results, it became evident that the flexibility in our approach, which allowed for silent periods in the signal, could reduce the strong emphasis on signal processing and signal detection steps in real-world scenarios. In other words, a relaxed window around the vibro-measurement vector, which signifies when the vibro-measurements break the noise floor and when it dies down, should be enough for the proposed algorithm to accurately localize occupant. It is a convenient improvement as in the employment of such localization systems, the event detection problem constitutes a major drawback.

The advancements made in vibro-localization techniques, as presented in this study, open up several promising avenues for further exploration. One potential direction is the integration of global optimization techniques to enhance the accuracy and robustness of localization. By leveraging such techniques, we could refine the estimation process, ensuring that the solution converges to a global minimum, thereby minimizing localization errors. Additionally, a joint solution approach that simultaneously addresses the location estimation problem and the BSE problem could be explored. Such a holistic approach would ensure that the system not only accurately

determines the location but also effectively handles unreliable sensor data in a unified framework. This could further streamline the process and potentially lead to real-time localization capabilities with higher reliability.

Chapter 4

Modeling and Analysis of Dispersive Propagation of Structural Waves for Vibro-Localization

The dispersion of structural waves, where wave speed varies with frequency, introduces significant challenges in accurately localizing occupants in a building based on vibrations caused by their movements. This study presents a novel multi-sensor vibro-localization technique that accounts for dispersion effects, enhancing the accuracy and robustness of occupant localization. The proposed method utilizes a model-based approach to parameterize key propagation phenomena, including wave dispersion and attenuation, which are fitted to observed waveforms. The localization is achieved by maximizing the joint likelihood of the occupant's location based on sensor measurements. The effectiveness of the proposed technique is validated using two experimental datasets: one from a controlled environment involving an aluminum plate and the other from a building-scale experiment conducted at Goodwin

Hall, Virginia Tech. Results for the proposed algorithm demonstrate a significant improvement in localization accuracy compared to benchmark algorithms. Specifically, in the aluminum plate experiments, the proposed technique reduced the average localization precision from 7.77 centimeters to 1.97 centimeters, representing a ∼74% improvement. Similarly, in the Goodwin Hall experiments, the average localization error decreased from 0.67 meters to 0.3 meters, with a ∼55% enhancement in accuracy. These findings indicate that the proposed approach outperforms existing methods in accurately determining occupant locations, even in the presence of dispersive wave propagation.

4.1 Introduction

Vibro-localization is an occupant localization method that employs the ambient measurements of structural waves generated by occupants' activities to determine their locations in a building. Vibro-localization is particularly useful in smart buildings, where the occupants' locations are used to improve the safety, security, and energy efficiency of the building. For instance, in an emergency situation, the occupants' locations can be used to guide them to safety, or to help the first responders to locate them. Another example is monitoring the gait parameters of the occupants, which can be used to detect the early signs of many neurodegenerative diseases such as Parkinson's disease, Alzheimer's disease, and multiple sclerosis [21, 22]. Various spatiotemporal characteristics of human gait, such as symmetry [20, 25, 32, 42] and gait variability [13, 23, 29], which can be obtained with vibro-localization techniques,

have been shown to be reliable indicators of neurodegenerative diseases.

Vibro-localization techniques are based on the premise that the structural waves generated by the occupants' activities propagate through the building's structure and are measured by a network of sensors, i.e., accelerometers. However, these waves are subject to various propagation phenomena, such as dispersion, attenuation, and reflection, which can transform the waveforms and introduce errors in the localization outcomes. Therefore, each sensor's measurement corresponds to a transformed version of the wave generated by the occupant, making the localization problem challenging. Dispersion is a particularly challenging phenomenon that affects the wave propagation in real-world settings, i.e., defined by a long propagation path, low-frequency waves, low spectral resolution, etc.

4.1.1 Relevant Literature

The literature in vibro-localization considering dispersion is diverse and spans various disciplines, including structural engineering, signal processing, and machine learning. In their work, Mirshekari et al. [44] proposed a localization technique that employs a two-fold strategy to mitigate the effect of dispersion on the localization outcomes: (1) Wavelet-based dispersion mitigation by narrow-band filtering; and (2) adaptive sensor selection to localize the occupant with closer sensors to reduce the effect of dispersion on the localization outcomes. In their later work, the authors extend their technique to accommodate the variability among the occupants [46] and disturbances along the propagation path [47]. The authors show that their technique

outperforms the traditional TDoA-based techniques in terms of localization accuracy and robustness as the perceived wave velocity is automatically deduced from the floor acceleration data collected by a sensor network.

Time-of-Arrival (ToA) of flexural waves in a dispersive medium exhibits a nonlinear dependence on the distance d, specifically proportional to $d^{4/3}$ [10]. The perceived velocity of the wave, v_p, at any given distance d from the source, is defined based on the ToA of the maximum signal envelope. This relationship is mathematically expressed as $v_p(d) = \frac{1}{\eta} d^{-1/3}$, where η is a constant that depends on the boundary conditions and material properties. This equation indicates that in a dispersive media, the flexural wave's perceived velocity v_p is not constant, but rather decreases nonlinearly as the distance d increases. In [10], Bahroun et al proposed a localization technique that employs the sign of the TDoA measurements to estimate the distance between the source and the sensor [10].

Alajlouni et al. [3] show that the dispersive nature of the floor manifests itself as an exponential relationship between the signal energy and the distance between the sensor and the source. By exploiting this relationship, the authors propose a localization technique that employs the signal energy measurements to estimate the distance between the source and the sensor, rather than solving for the ToA of the waves, or the TDoA among the sensors. In their later work, the authors extend this technique to accommodate the measurement uncertainty. Their MLE-based technique estimates the distance between the source and the sensor by maximizing the likelihood of the observed signal energy measurements [3]. The authors show that their technique outperforms the traditional energy-based techniques in terms of

localization accuracy and robustness.

Ambarkutuk et al. [7] propose an information-theoretic approach to mitigate the effects of the dispersion on the localization outcomes. The authors show that measurement uncertainty and dispersion may render some of the sensors as Byzantine, i.e., their measurements are not informative, or faulty, about the source location. The authors propose a sensor fusion technique that eliminates the Byzantine sensors from the network, and maximize the joint likelihood of occupant location given the sensor measurements.

MejiaCruz et al. [41] utilize a probabilistic approach to estimate a transfer function and force shape; thereby, localizing events based on structural vibrations measurements. Their algorithm, called Probabilistic Force Estimation and Event Localization (PFEEL), involves three main stages: (1) probabilistic transfer function estimation; (2) probabilistic force estimation; and, (3) event localization. It uses sensor data to measure vibration waves and applies probabilistic methods to accurately estimate forces and locate events within a structure. In their later work [42], the authors extend the PFEEL algorithm by representing the transfer functions as stochastic processes. This extension allowed the authors to better gauge the uncertainty in the estimated transfer functions and improve the accuracy of the force estimation and event localization.

4.1.2 Challenges in Vibro-Localization

Several challenges exist in the current approaches to vibro-localization:

1. *The sensors are not ideal.* Measurement uncertainty is a crucial factor that contributes to the localization error. [3] assumes a normal distribution of the signal energy measurements to address this. The maximum likelihood solution under the normality assumption yields to a convex optimization landscape. However, due to the complex nature of wave propagation in real-world settings, this assumption rarely holds true. Therefore, the gradient-based solvers may not converge to the global optimum, leading to suboptimal localization results.

2. *The dynamics are complex.* Wave propagation is a complex dynamic phenomenon influenced by various factors, such as dispersion, attenuation, and material inhomogeneities. For instance, [36, 37, 44] assume a constant wave speed to estimate temporal parameters of the wave, such as the ToA or the TDoA. However, reducing the problem to a single parameter estimation, i.e., group velocity, may not be sufficient to capture the complexity of wave propagation in structures. The wave speed can vary depending on several factors, including the material properties of the floor and the frequency of the waves, leading to potential errors in localization accuracy. [10] assume that the wave speed is solely a function of propagation distance. However, this assumption may oversimplify the complex nature of wave propagation in real-world settings, where wave speed can be influenced by other factors, such as frequency-dependent dispersion and material inhomogeneities.

3. *Each footstep is different.* Ground reaction forces generated by footsteps can vary significantly depending on the individuals' gait characteristics, such as step length, step width, and walking speed. This variability can introduce

errors in the localization results as the technique may not accurately capture the unique characteristics of each individual's footsteps.

4. *Forcing is unknown.* Vibro-localization techniques often require the estimation of the force shape generated by the occupant's footsteps [17, 41, 42]. This force shape is used to estimate the transfer function between forcing and sensor measurements. However, estimating the force shape accurately can be challenging as it depends on various factors, such as the individual's gait characteristics, the material properties of the floor, and the frequency of the waves. Inaccurate force estimation can lead to errors in the localization results, as the technique may not accurately model the wave propagation through the floor.

5. *The propagation is a rapid phenomenon relative to sampling.* Footsteps generate fast and repetitive signals, leading to a situation where there are insufficient samples to fully capture the wave characteristics at reasonable sampling rates. As a result, transfer function estimates often suffer from low spectral resolution. For instance, [41] employs cross- and auto-spectral density of the measurement vectors to estimate the transfer function of the propagation phenomena. However, the limited frequency resolution and the presence of measurement uncertainty, can significantly hinder the accuracy of these estimates and, consequently, the localization results.

4.1.3 Summary of the Contributions

This chapter introduces a vibro-localization technique that determines occupants' locations in a building using structural vibration waves, bypassing force estimation. The method simplifies this localization process by employing a model-based approach to represent key propagation phenomena such as dispersion and attenuation, which are parameterized and fitted to measured waveforms. The estimated occupant location is then derived from the joint likelihood function of all sensor measurements.

Our work builds on previous research and makes the following contributions:

- *Multi-Sensor Perception* (addresses challenge 1): We propose a multi-sensor technique that aggregates information from multiple sensors, bypassing the assumption of normal distribution in signal energy measurements. The averaging during the signature estimation does not assume anything about the underlying error distributions, making it more robust to real-world complexities and variabilities.

- *Enhanced Wave Propagation Modeling* (addresses challenges 2, 3, and, 4): We propose a model-based approach that accurately captures the dispersive and attenuative properties of structural vibration waves focusing on key parameters like wave speed and attenuation coefficient. This approach improves localization accuracy by avoiding oversimplifications.

- *A Parametric Approach to Modeling the Physical Properties* (addresses challenge 5): We introduce a piecewise constant velocity profile modeling the dis-

persion mechanism that can be used to estimate the occupant location, even with low-spectral resolution in the transfer function estimates. In the calibration of the vibro-localizer, the wave velocity and attenuation coefficient are estimated by fitting the transfer function to the measured waveforms.

4.1.4 Organization of the Chapter

The rest of the chapter is organized as follows. In Section 4.2, we detail the proposed vibro-localization technique, including the forward problem of wave propagation and the inverse problem of estimating the occupant's location using structural vibrations. Section 4.3 presents the experimental validation of the proposed method through controlled plate experiments and building-scale experiments in Goodwin Hall, Virginia Tech. The results demonstrate the effectiveness and improved accuracy of our technique compared to existing methods. Finally, in Section 4.4, we conclude the chapter by summarizing the key findings and discussing potential directions for future research in the field of vibro-localization.

4.2 Methodology

This section presents the proposed vibro-localization technique in greater detail. The localization loss function is derived from the wave propagation model, and the unpropagation operator is used to recover the original waveform.

The proposed technique leverages the structural vibration waves induced by an oc-

cupant's footsteps and captured by a network of sensors distributed throughout the building. The vibro-localization technique estimates the occupant's location probabilistically by assigning a probability to a location vector, representing the likelihood of the occupant's presence at that location. The technique is based on our proposed wave propagation model. The concepts of the propagation and unpropagation operators are used to model the wave transmission and recovery processes, respectively. This technique involves estimating the signature waveform induced by the occupant's footsteps and comparing it with the reconstructed waveforms at the sensors to estimate the occupant's location.

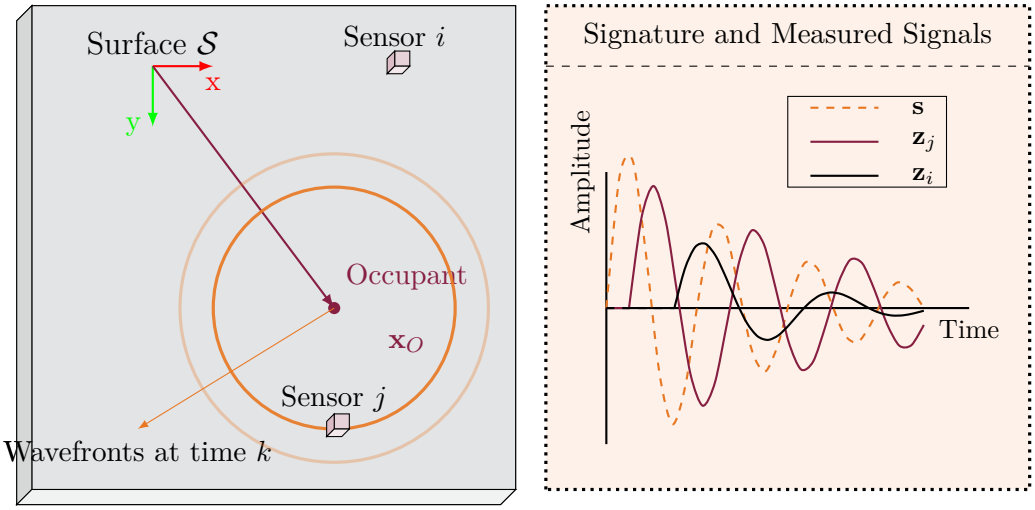

Figure 4.1: This figure illustrates the wave propagation process. **Left:** An illustration of the geometric layout of the floor, sensors, and the occupant location. **Right:** The wave propagation process from the occupant to the sensors. As can be seen in the figure, both sensors i, j are affected by the wave propagation process. Sensor i is further away to the occupant than sensor j, which results in a delay and more attenuation relatively to sensor j.

4.2.1 Forward Problem: Wave Propagation

Consider a homogeneous and isotropic floor surface $\mathcal{S} \subset \mathbb{R}^2$ of a building. When an occupant O steps at a location $\mathbf{x}_O \in \mathcal{S}$, they induce a distinct waveform vector $\mathbf{s} = (s[0], \ldots, s[K-1])^\top \in \mathbb{R}^K$ at that location, where K denotes the total number of discrete time samples in the waveform, with each element $s[k]$ corresponding to the recorded signal at time step k. This waveform $\mathbf{s}$, is referred as *the signature*, and it propagates through the floor and is detected by stationary sensors placed at various positions $\mathbf{x}_{S,i} \in \mathcal{S}$, for $i \in \mathcal{I} = \{0, \ldots, M-1\}$.

The wave propagation process is illustrated in Figure 4.1. The wave generated by the occupant's footsteps travels through the floor and is detected by the sensors. For sensor i, the observed waveform $\mathbf{z}_i = (z_i[0], \ldots, z_i[K-1])^\top \in \mathbb{R}^K$ is a transformed version of the original waveform due to the effects of propagation. The variations in the observed waveforms $\mathbf{z}_i$ among different sensors arise from the different propagation paths taken by the wave from the occupant to each sensor.

The transformation in the observed waveform $\mathbf{z}_i$ is primarily caused by three factors: dispersion, attenuation, and geometric spreading. Dispersion refers to the phenomenon where the phase velocity of the wave varies with its frequency, resulting in a frequency-dependent phase delay $\tau(\omega)$ in the waveforms. This phase delay can be expressed as:

$$\tau(\omega) = \exp\left(-j\omega \frac{d}{v(\omega)}\right) ,$$

where $d = \|\mathbf{x}_O - \mathbf{x}_{S,i}\|$ represents the distance between the occupant's location $\mathbf{x}_O[k]$ and the sensor location $\mathbf{x}_{S,i}$, and $v(\omega)$ is the phase velocity at frequency ω. Atten-

uation represents the decrease in amplitude of the wave as it travels through the medium. It can be characterized by:

$$a = \exp(-\eta_a d) \ ,$$

where η_a is the attenuation coefficient. Geometric spreading accounts for the reduction in amplitude due to the wave spreading over a larger area as it propagates. This effect is expressed as:

$$g = \begin{cases} \min\{1, \frac{1}{\sqrt{d}}\} & \text{if } d > 3\lambda \\ 1 & \text{otherwise} \end{cases} \ .$$

Together, attenuation a and geometric spreading g determine how the energy of the wave is distributed and dissipated over the propagation distance d. Dispersion, on the other hand, introduces a frequency-dependent phase delay $\tau(\omega)$ in the waveforms, causing the wave to spread out in time.

To succinctly represent the propagation process, we define the propagation operator P and its inverse P^{-1}. The operator P models the forward wave transmission, while P^{-1} represents the process of recovering the original waveform $\mathbf{s}$ from the observed data $\mathbf{z}_i$. These operators provide a simplified and systematic approach to analyzing waveforms in the vibro-localization technique. The propagation operator P is defined mathematically as:

$$\mathbf{z}_i = P\left(\mathbf{s}; \mathbf{x}, \mathbf{x}_{S,i}\right) = a\, g\, \mathcal{F}^{-1}\left\{\tau(\omega)\mathcal{F}\left\{\mathbf{s}\right\}\right\},$$

where $\mathcal{F}$ and $\mathcal{F}^{-1}$ represent the Fourier transform and its inverse, respectively. The unpropagation operator P^{-1} is defined as:

$$P^{-1}\left(\mathbf{z}_i; \mathbf{x}, \mathbf{x}_{S,i}\right) = \frac{1}{a\, g}\, \mathcal{F}^{-1}\left\{ \frac{1}{\tau(\omega)} \mathcal{F}\left\{\mathbf{z}_i\right\} \right\},$$

where the inverse operation recovers the original waveform $\mathbf{s}$ from the observed data $\mathbf{z}_i$.

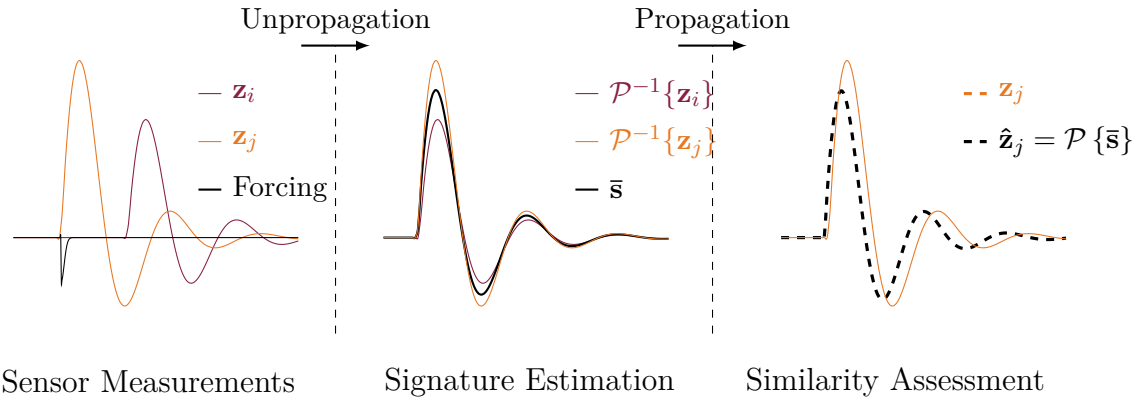

Figure 4.2: The figure illustrates the process of transforming sensor measurements, $\mathbf{z}_i$ and $\mathbf{z}_j$, into estimated signatures and assessing their similarity. The shorthand P denotes the propagation operator, which is used to convert sensor data into meaningful signatures. Initially, the unpropagation step transforms the measurements into estimated signatures $\mathcal{P}^{-1}\{\mathbf{z}_i\}$ and $\mathcal{P}^{-1}\{\mathbf{z}_j\}$, producing the estimated signature $\bar{\mathbf{s}}$. Subsequently, the similarity between the propagated signature $\mathcal{P}\{\bar{\mathbf{s}}\}$ and the original measurement $\mathbf{z}_j$ is assessed, allowing for a comparison of the sensor outputs.

4.2.2 Inverse Problem: Vibro-Localization

The vibro-localization technique aims to estimate the occupant's position based on the structural vibrations generated by their footsteps and captured by the sensor network. This method relies on reconstructing the original waveform induced by the occupant's steps and comparing it with the waveforms observed by the sensors.

As illustrated in Figure 4.2, the proposed algorithm first computes the average waveform $\bar{\mathbf{s}}(\mathbf{x})$ at each candidate location $\mathbf{x}$ using the unpropagation operator.

$$\bar{\mathbf{s}}(\mathbf{x}) = \frac{1}{M} \sum_{i \in \mathcal{I}} \mathcal{P}^{-1}\{\mathbf{z}_i, \mathbf{x}, \mathbf{x}_{S,i}\} \ .$$

This average waveform $\bar{\mathbf{s}}(\mathbf{x})$ represents the expected waveform at the candidate location $\mathbf{x}$, averaged over all sensors. Following this, the estimated waveform $\hat{\mathbf{z}}_i(\mathbf{x}) = \mathcal{P}\{\bar{\mathbf{s}}(\mathbf{x}); \mathbf{x}; \mathbf{x}_{S,i}\}$ at each sensor location $\mathbf{x}_{S,i}$ is computed by propagating the average waveform $\bar{\mathbf{s}}(\mathbf{x})$ back to the sensor location $\mathbf{x}_{S,i}$ for all sensors.

Next, we employ the cosine similarity index between the measurement vector $\mathbf{z}_i$ and the estimated waveform $\hat{\mathbf{z}}_i(\mathbf{x})$ to quantify the temporal alignment and scale mismatch between the observed and estimated waveforms. The similarity index, r_i, that quantifies the agreement between the observed and estimated waveforms at sensor i is defined as:

$$r_i(\mathbf{x}) = \mathbf{z}_i \cdot \hat{\mathbf{z}}_i(\mathbf{x}) \ ,$$

where $\cdot$ denotes the dot product between two waveforms. Aggregating the similarity indices over all sensors, we obtain the similarity vector $\mathbf{r}(\mathbf{x}) = (r_0(\mathbf{x}), \ldots, r_{M-1}(\mathbf{x}))^\top$.

Consequently, the similarity vector $\mathbf{r}$ quantifies the agreement between the observed and estimated waveforms at each sensor. One might consider the similarity vector $\mathbf{r}$ as a feature vector that characterizes the likelihood of the occupant's presence at a given location $\mathbf{x}$.

An optimization algorithm can be used to solve for the location vector $\mathbf{x}$ that maximizes the similarity vector $\mathbf{r}$. We formulate this optimization problem as a probabilistic model, where the similarity index $r_i(\mathbf{x})$ are used to compute the likelihood of the occupant's presence at each location. The similarity index $r_i(\mathbf{x})$ is evaluated for all locations in the localization space $\mathcal{S}$ and then normalized using a softmax function to convert the similarity scores into probabilities, representing the likelihood of the occupant's presence at each location. The likelihood function $f_i(\mathbf{x})$ at location $\mathbf{x}$ for sensor i is defined as:

$$f_i(\mathbf{x}) = \frac{\exp(r_i(\mathbf{x}))}{\sum_{\mathbf{x'} \in \mathcal{S}} \exp(r_i(\mathbf{x'}))} \ .$$

Finally, the occupant's estimated location $\hat{\mathbf{x}}_O$ is determined by maximizing the product of the likelihood functions over all sensors, i.e., the joint likelihood:

$$\hat{\mathbf{x}}_O = \underset{\mathbf{x} \in \mathcal{S}}{\operatorname{argmax}} \prod_{i \in \mathcal{I}} f_i(\mathbf{x}) \ .$$

This probabilistic approach allows the vibro-localization technique to estimate the occupant's location by integrating information from multiple sensors, leveraging the unique propagation characteristics of the structural waves in the building.

Algorithm 4.1 Vibro-Localization Algorithm

procedure VIBROLOCALIZATION($\{\mathbf{z}_i\}_{i=0}^{M-1}, \{\mathbf{x}_{S,i}\}_{i=0}^{M-1}, \mathcal{S}, v(\omega), \eta_a$)
  $\hat{\mathbf{x}}_O \leftarrow$ null
  for all candidate locations $\mathbf{x} \in \mathcal{S}$ **do** ▷ `Unpropagate the measured signals to estimate the source waveform`
    for all $i \in \{0, 1, \ldots, M-1\}$ **do**
      $\mathbf{s}_i(\mathbf{x}) \leftarrow P^{-1}(\mathbf{z}_i; \mathbf{x}, \mathbf{x}_{S,i})$
    end for ▷ `Compute the average source waveform across all sensors`
    $\bar{\mathbf{s}}(\mathbf{x}) \leftarrow \frac{1}{M} \sum_{i=0}^{M-1} \mathbf{s}_i(\mathbf{x})$ ▷ `Propagate the average source waveform back to each sensor and compute similarity indices`
    for all $i \in \{0, 1, \ldots, M-1\}$ **do**
      $\hat{\mathbf{z}}_i(\mathbf{x}) \leftarrow P\left(\bar{\mathbf{s}}(\mathbf{x}); \mathbf{x}, \mathbf{x}_{S,i}\right)$
      $r_i(\mathbf{x}) \leftarrow \mathbf{z}_i^\top \hat{\mathbf{z}}_i(\mathbf{x})$
    end for ▷ `Compute the likelihood function at location` $\mathbf{x}$
    $f(\mathbf{x}) \leftarrow \prod_{i=0}^{M-1} \frac{\exp\left(r_i(\mathbf{x})\right)}{\sum_{\mathbf{x}' \in \mathcal{S}} \exp\left(r_i(\mathbf{x}')\right)}$
  end for ▷ `Estimate the occupant's location by maximizing the joint likelihood`
  $\hat{\mathbf{x}}_O \leftarrow \arg\max_{\mathbf{x} \in \mathcal{S}} f(\mathbf{x})$
  return $\hat{\mathbf{x}}_O$
end procedure

Figure 4.2 and Algorithm 4.1 illustrate the core process of the proposed vibro-

localization algorithm, focusing on how sensor measurements are transformed and used to estimate the occupant's location. The algorithm begins by collecting measurements $\mathbf{z}_i$ and $\mathbf{z}_j$ from sensors located at positions $\mathbf{x}_{S,i}$ and $\mathbf{x}_{S,j}$, respectively. These measurements capture the structural vibrations caused by the occupant's footsteps. To estimate the original waveform generated at a candidate location $\mathbf{x}$, the algorithm applies the unpropagation operator $\mathcal{P}^{-1}$ to each sensor's measurement. This process effectively reverses the effects of wave propagation—including dispersion and attenuation—yielding estimated source signatures $\mathcal{P}^{-1}\{\mathbf{z}_i\}$ and $\mathcal{P}^{-1}\{\mathbf{z}_j\}$.

These individual estimated signatures are then aggregated by computing their average, resulting in a more robust estimate of the source waveform $\bar{\mathbf{s}}$. Averaging mitigates the impact of noise and sensor-specific anomalies, enhancing the reliability of the estimated signature. Next, the propagation operator $\mathcal{P}$ is applied to $\bar{\mathbf{s}}$ to simulate how this average signature would appear at each sensor location if it originated from the candidate location $\mathbf{x}$. This generates propagated signatures $\mathcal{P}\{\bar{\mathbf{s}}\}$ that can be directly compared to the original sensor measurements $\mathbf{z}_i$ and $\mathbf{z}_j$. By assessing the similarity between the propagated signatures and the actual measurements—typically using the dot product or another similarity metric—the algorithm quantifies how well the candidate location explains the observed data. Repeating this process across all candidate locations allows the algorithm to construct a likelihood map, ultimately estimating the occupant's location as the point that maximizes the joint likelihood function.

4.3 Results

In this section, we present the results of the proposed technique for both the plate and building datasets. The results are presented in terms of accuracy and precision of the localization estimates. These results are described in detail for each dataset, including the statistical analysis of the localization error and the empirical PDF and CDF of the localization errors.

4.3.1 Plate Experiments

Figure 4.3 shows a representative result from the dataset where the impact location is close to the sensor array.

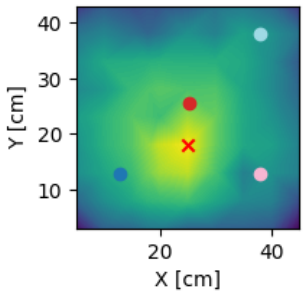

(a) Joint likelihood of the baseline method [41]

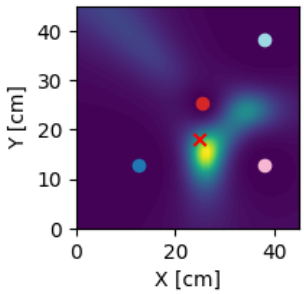

(b) Joint likelihood of the proposed method

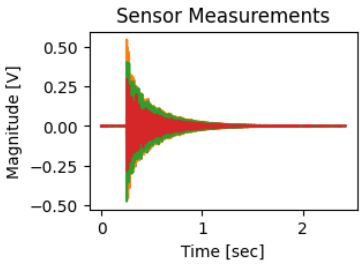

(c) Sensor Measurements

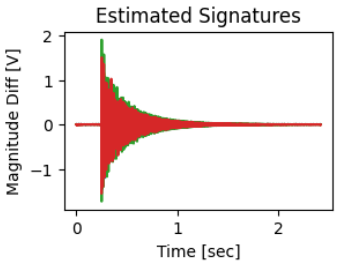

(d) Estimated Signatures

Figure 4.3: The figure presents a comparison of the joint likelihoods and sensor data for an impact location near the sensor array. The top left subfigure shows the joint likelihood computed using the proposed method, while the top right subfigure displays the joint likelihood obtained from the baseline method as described in [41]. The bottom left subfigure illustrates the raw sensor measurements, and the bottom right subfigure shows the estimated signatures derived from these measurements. This comparison highlights the performance of both methods in accurately estimating the impact location based on vibrational data.

Table 4.1 provides a detailed statistical descriptives of the localization error such as mean, standard deviation, median, and Mean Absolute Deviation (MAD). The (winsorized-) mean and median are the measures of accuracy, while the standard deviation and MAD are the measures of precision, i.e., the spread. The results show that the proposed technique estimated the impact locations with a mean localization

error of 18.01 cm and a standard deviation of 1.97 cm. In contrast, the baseline technique reported in [41] exhibited a mean localization error of 19.19 cm with a standard deviation of 7.77 cm. This difference indicates that the proposed technique has shown improvement over the baseline without using the hammer impact information as used in [41].

	Raw		Winsorized (at 10 cm)		Rank-Based	
	Mean	Std. Dev.	Mean	Std. Dev.	Median	MAD
Baseline [41]	19.19	7.77	16.34	5.48	19.13	5.43
Proposed	**18.01**	**1.97**	**17.66**	**1.04**	**17.08**	**0.34**

Table 4.1: Statistical analysis of localization error for the baseline method [41] and the proposed technique. The table compares the accuracy and precision of these techniques. The proposed technique consistently demonstrates lower mean error and variability across all metrics, indicating improved accuracy and robustness compared to the baseline. The reduction in standard deviation and MAD for the proposed method highlights its stability and resistance to outliers in the dataset.

The empirical PDF and CDF of the localization errors provide further insights into the performance of the proposed technique. Comparing the CDF curves between the proposed and baseline techniques can highlight differences in the overall error distribution. Figure 4.4 demonstrates the empirical PDF and CDF of the localization errors for the proposed and baseline techniques. As can be seen in the figure, the proposed technique shows a sharper peak in the PDF curve, indicating a higher frequency of small errors relative to the baseline which demonstrated a broader distribution over the range of localization errors. The CDF curve for the proposed technique exhibits a steeper incline at lower error values, suggesting that a signifi-

cant portion of the errors are small, which is desirable for high-accuracy localization systems. In contrast, the baseline technique shows a more gradual increase in the CDF curve.

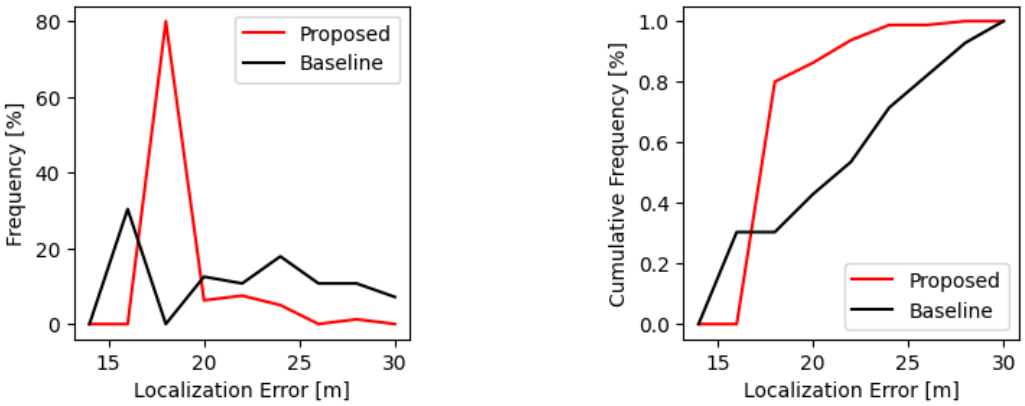

(a) PDF (b) CDF

Figure 4.4: PDF and CDF of localization error for the proposed method and the baseline approach. In the PDF (left), the proposed method exhibits a sharp peak around 20 meters, indicating a higher frequency of lower localization errors compared to the baseline, which shows a more distributed error profile. The CDF (right) further supports this observation, as the proposed method achieves 80% cumulative frequency at a lower error range than the baseline, demonstrating a more consistent and accurate performance. These results suggest that the proposed technique significantly reduces localization error, achieving more reliable estimates than the baseline method.

4.3.2 Building Scale Experiments with Dispersive Propagation

Figure 4.5 illustrates three representative results observed in the building dataset. The figure shows the joint likelihood of the proposed technique as well as estimated

impact locations. In an ideal scenario, the joint likelihood function should have a single peak at the true impact location with minimal uncertainty. Figures 4.5a to 4.5c demonstrate a scenario an occupant is walking along the corridor, and the sensors are placed at different locations to capture the vibrations. Figure 4.5a demonstrates the scenario where the occupant is located at the leftmost end of the corridor while Figure 4.5b shows the scenario where the occupant is located at the center of the corridor. Finally, Figure 4.5c illustrates the scenario where the occupant is located at the rightmost end of the corridor. The results demonstrate that the proposed technique accurately estimated the impact locations for both occupants.

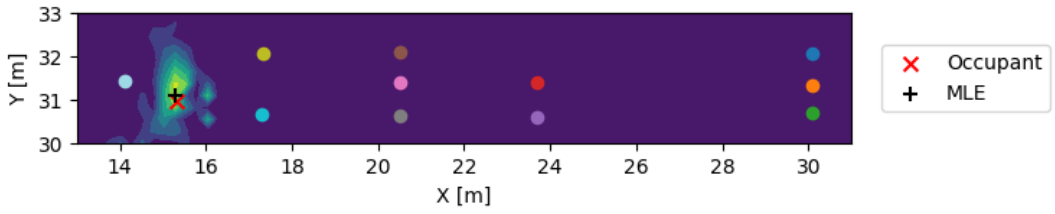

(a)

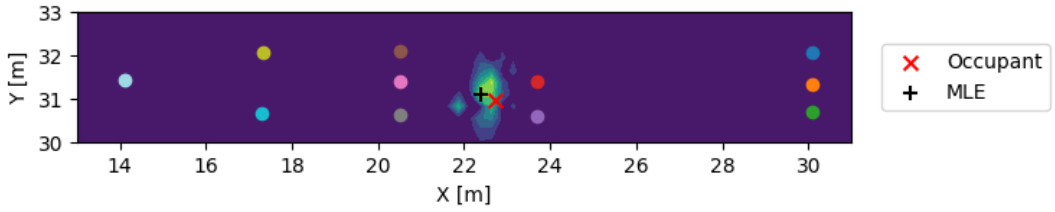

(b)

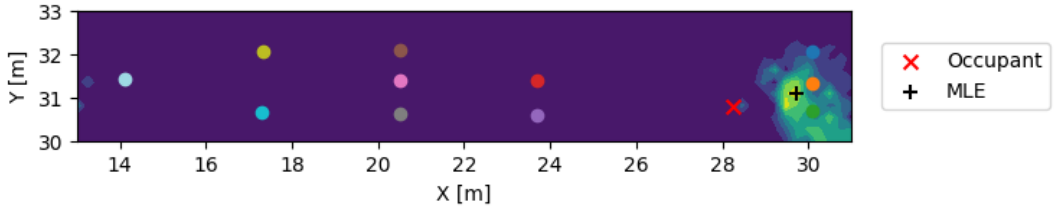

(c)

Figure 4.5: This figure presents three representative examples of the localization results obtained using the proposed method on the building dataset. Each subfigure displays the joint likelihood calculated from the measured waveforms, where the true occupant location is indicated by a red cross (×) and the estimated location by a black plus sign (+). Figure 4.5a shows the scenario where the occupant is positioned at the leftmost end of the corridor, Figure 4.5b depicts the occupant at the center, and Figure 4.5c illustrates the occupant at the rightmost end. The results indicate that the proposed technique reliably estimates the impact locations, demonstrating its effectiveness across different occupant positions.

Localization accuracy was evaluated by comparing the estimated impact locations with the ground truth locations. We employed the mean of the joint likelihood function as the estimated impact location, which was then compared to the ground truth location to calculate the localization error. Table 4.2 demonstrates the comparative analysis of the proposed and baseline techniques in terms of localization error. The results demonstrate that the proposed technique estimated the impact locations with an RMSE of 0.49 and 0.71 meters for occupant A and B, respectively. On the other hand, the baseline, which was reported in [4], exhibited an RMSE of 0.89 and 0.94 meters for occupant A and B, respectively. This indicates that the proposed technique significantly improves the baseline results in terms of localization accuracy.

	Occupant-A			Occupant-B		
	RMSE x	RMSE y	RMSE $\|\cdot\|$	RMSE x	RMSE y	RMSE $\|\cdot\|$
Baseline [4]	0.67	0.58	0.89	0.74	0.58	0.94
Proposed	**0.3**	**0.31**	**0.49**	**0.67**	**0.24**	**0.71**

Table 4.2: Comparative analysis of localization error for Occupant A and Occupant B using the proposed and baseline methods. The table presents the RMSE in both the x- and y-coordinates, as well as the overall magnitude of the RMSE for each position. The proposed method demonstrates a significant reduction in localization error across all metrics for both occupants.

Table 4.3 presents descriptive statistics of localization error for Occupant-A and Occupant-B using three error estimates considering the outliers in the data: raw, Winsorized at 1 meter, and rank-based methods. For the raw data, Occupant-A shows a mean localization error of 0.35 meters with a standard deviation of 0.21 meters, while Occupant-B exhibits higher error values, with a mean of 0.62 meters and a

larger standard deviation of 1.06 meters. After Winsorizing at 1 meter, Occupant-A's mean error slightly decreases to 0.34 meters with a reduction in standard deviation to 0.2 meters, and Occupant-B's mean error decreases to 0.48 meters with a reduction in standard deviation to 0.29 meters. This suggests that extreme values had more influence on Occupant-B in the raw data. The rank-based method, which uses median and MAD, provides a more robust central tendency, with Occupant-A showing a median error of 0.31 meters and a MAD of 0.12 meters, while Occupant-B has a median of 0.4 meters with a MAD of 0.19 meters. Additionally, the 95% confidence interval for the mean localization error is (0.31, 0.38) meters for Occupant-A and (0.44, 0.80) meters for Occupant-B, indicating that Occupant-B consistently shows higher localization error estimates across all metrics, although variability is reduced when outliers are controlled.

	Raw		Winsorized (at 1 meters)		Rank-Based	
	Mean	Std. Dev.	Mean	Std. Dev.	Median	MAD
Occupant-A	0.35	0.21	0.34	0.2	0.31	0.12
Occupant-B	0.62	1.06	0.48	0.29	0.4	0.19

Table 4.3: Descriptive statistics of localization error for Occupant A and Occupant B using the proposed technique, across different data treatment methods: raw data, Winsorized data (at 1 meter), and rank-based data. The results indicate that Occupant A consistently shows lower localization error across all methods compared to Occupant B, with smaller variability. The Winsorized and rank-based methods further reduce the impact of outliers, particularly for Occupant B, where both the mean error and variability are notably reduced. This suggests that the proposed technique is more robust and stable when outliers are controlled, providing more reliable localization estimates.

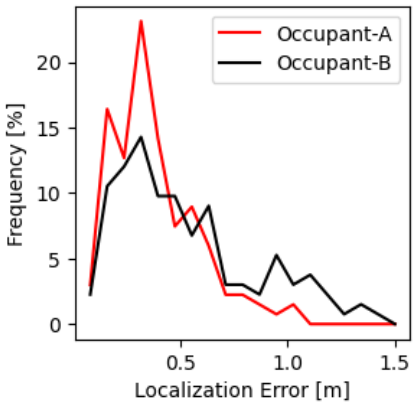

(a) PDF of the localization error observed in Occupant A and Occupant B data

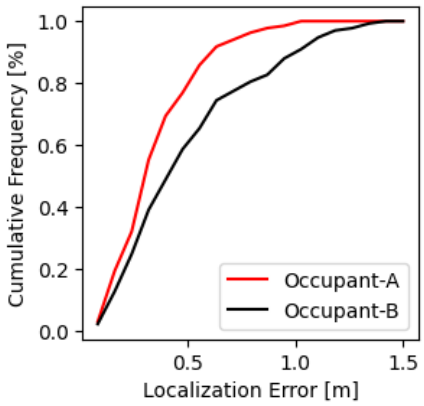

(b) CDF of the localization error observed in Occupant A and Occupant B data

Figure 4.6: PDF and CDF of the localization error for both occupants in the Goodwin Hall dataset. The results indicate that the error distributions for both Occupant A and Occupant B are similar, demonstrating that the proposed technique is robust to inter-occupant differences. Despite the variations in walking patterns and body dynamics between different individuals, the method maintains relatively consistent performance.

The empirical PDF and CDF of the localization errors shown in Figure 4.6 provides additional insights into the performance of the proposed technique. The empirical PDF illustrates the distribution of localization errors, allowing us to observe the concentration of errors around certain values. A sharp peak in the PDF indicates a high frequency of small errors, suggesting that the proposed method consistently achieves close proximity to the true location. Conversely, a broader distribution might indicate greater variability in localization accuracy. The empirical CDF, on the other hand, offers a cumulative perspective by showing the proportion of errors that fall below a certain threshold. A steep incline in the CDF curve at lower error values reflects that a significant portion of the errors are small, which is desirable for high-

accuracy localization systems. Comparing the CDF curves between the proposed and baseline techniques can reveal differences in the overall error distribution, indicating whether the proposed method consistently outperforms the baseline across the entire range of localization errors or only in specific scenarios.

4.4 Conclusions

This chapter introduced a novel method for characterizing and localizing occupants in a building by analyzing structural vibration waves generated by their activities. The proposed approach utilized the wave equation, incorporating key properties such as dispersion and attenuation, to propagate and unpropagate the waves. These properties were estimated from waveforms recorded by sensors placed at various locations in the building. Our experimental validation demonstrated that the method accurately captures the propagation and unpropagation of waves, enabling precise localization of the occupants.

The method was applied to two experimental datasets: a controlled aluminum plate test and a building-scale experiment. The results showed that the proposed technique outperforms existing methods by significantly reducing localization error. For example, in the plate experiment, the proposed method achieved a mean localization error of 18.01 cm with a standard deviation of 1.97 cm, compared to the baseline technique's mean error of 19.19 cm and standard deviation of 7.77 cm. Similarly, in the building-scale experiment, the method estimated impact locations with an RMSE of 0.49 meters for Occupant A and 0.71 meters for Occupant B, in contrast

to the baseline's RMSE of 0.89 meters and 0.94 meters, respectively.

Furthermore, the proposed technique does not require prior knowledge of the force exerted by the occupants, and learns the dispersive nature of the floor from a training dataset. This feature makes the method more versatile and applicable to a wider range of scenarios, where the force information is not readily available. Also, the method demonstrated robustness to occupant differences, as similar error distributions were observed for both occupants, underscoring the method's adaptability to varying walking patterns and footstep characteristics. Vibro-localization is a challenging problem that becomes more difficult as the propagation path becomes longer due to dispersion. With the proposed technique, we were able to accurately estimate the impact locations even in the presence of dispersive propagation, as demonstrated in the building-scale experiment.

In conclusion, this work advances vibro-localization by introducing a model-based approach that accurately represents key propagation phenomena such as dispersion and attenuation. The results demonstrate the technique's improved accuracy and precision, offering a significant contribution to fields such as structural health monitoring, activity recognition, and security monitoring, where reliable localization of vibration sources is essential.

Chapter 5

Conclusions and Future Work

5.1 Conclusions

This dissertation provides a comprehensive examination of vibro-localization within indoor environments, contributing valuable insights to the field of IOL. The initial chapters established the research objectives and highlighted the significance of vibro-localization as a cost-effective and privacy-conscious alternative to traditional localization methods.

In Chapter 2, the focus was directed towards the localization of individual steps using a single sensor. This chapter introduced methodologies aimed at enhancing the accuracy of detecting and localizing footsteps, addressing critical challenges associated with sensor precision and measurement uncertainties.

Chapter 3 expanded the scope by exploring the localization of individual steps through the integration of multiple sensors. The use of multiple accelerometers demonstrated a notable improvement in localization accuracy and reliability. By aggregating data from several sensors, the research mitigated the impact of individual sensor imperfections and environmental variabilities, thereby reinforcing the

robustness of the localization system.

Chapter 4 addressed the complexities introduced by dispersive wave propagation in vibro-localization. The chapter presented advanced signal processing techniques that effectively modeled and compensated for the dispersive characteristics of structural waves. This enhancement facilitated more precise multi-step localization, accommodating the intricate dynamics of wave propagation in various indoor settings.

Overall, this dissertation advances the field of indoor localization by systematically addressing the challenges inherent in single and multi-sensor systems. The methodologies developed and validated through empirical studies offer a solid foundation for future research and practical applications in smart environments. The findings underscore the potential of vibro-localization to achieve high levels of accuracy and efficiency, paving the way for its integration into diverse indoor tracking systems.

5.2 Future Work

Building on the foundational work presented in this dissertation, future research will focus on several key areas to further enhance vibro-localization technologies:

- **Multi-Resolution Decomposition Methodology**: Develop advanced techniques for separating vibration measurements into distinct events. This will enable more detailed analysis and improve localization precision by isolating relevant vibrational patterns from background noise.

- **Pyramid-Structured Feature Extraction**: Create sophisticated feature extraction algorithms that generate pyramid-structured features. These features will enhance the detection and analysis of complex vibrational patterns, facilitating the distinction between different types and intensities of movements.

- **Non-Maximal Suppression Techniques**: Develop non-maximal suppression algorithms to eliminate false positives generated during peak detection. This enhancement will improve the reliability of the localization system by ensuring that only genuine footsteps contribute to localization calculations.

- **Robust Bounding-Box Merging**: Design robust bounding-box merging algorithms to eliminate false positives in the interval-detection process. This will ensure more accurate tracking by consolidating relevant detection events and minimizing erroneous entries.

- **Scalability and Real-World Implementation**: Investigate the scalability of the proposed vibro-localization techniques for large-scale indoor environments. This includes optimizing sensor placement, data processing algorithms, and system integration to ensure practical applicability in real-world settings such as smart homes, healthcare facilities, and commercial buildings.

- **Privacy and Security Enhancements**: Continue to prioritize privacy and security by developing methods that further anonymize occupant data and protect against unauthorized access. Ensuring ethical standards will be paramount as vibro-localization technologies become more widespread.

These future research directions aim to refine and expand the capabilities of vibro-localization systems, enhancing their accuracy, reliability, and applicability in diverse indoor environments. By addressing these key areas, subsequent studies will contribute to the advancement of smart indoor tracking technologies, fostering innovations that benefit various application domains.

Bibliography

[1] Sa'ed Alajlouni and Pablo Tarazaga. A new fast and calibration-free method for footstep impact localization in an instrumented floor. *Journal of Vibration and Control*, 25:1629–1638, 5 2019. ISSN 1077-5463. doi: 10.1177/1077546319829943. URL http://journals.sagepub.com/doi/10.1177/1077546319829943.

[2] Sa'ed Alajlouni and Pablo Tarazaga. A passive energy-based method for footstep impact localization, using an underfloor accelerometer sensor network with kalman filtering. *Journal of Vibration and Control*, 26(11-12):941–951, 2020.

[3] Sa'ed Alajlouni, Jonathan Baker, and Pablo Tarazaga. Maximum likelihood estimation for passive energy-based footstep localization. *Mechanical Systems and Signal Processing*, 163, 1 2022. ISSN 10961216. doi: 10.1016/j.ymssp.2021.108158.

[4] Sa'ed Alajlouni and Pablo Tarazaga. A passive energy-based method for footstep impact localization, using an underfloor accelerometer sensor network with kalman filtering. *JVC/Journal of Vibration and Control*, 26:941–951, 6 2020. ISSN 17412986. doi: 10.1177/1077546319890520.

[5] Sa'ed Alajlouni, Mohammad Albakri, and Pablo Tarazaga. Impact localization in dispersive waveguides based on energy-attenuation of waves with the traveled distance. *Mechanical Systems and Signal Processing*, 105:361–376,

5 2018. ISSN 08883270. doi: 10.1016/j.ymssp.2017.12.007. URL https://linkinghub.elsevier.com/retrieve/pii/S0888327017306428.

[6] Fakhrul Alam, Nathaniel Faulkner, and Baden Parr. Device-free localization: A review of non-rf techniques for unobtrusive indoor positioning, 3 2021. ISSN 23274662.

[7] Murat Ambarkutuk, Sa'ed Alajlouni, Pablo A. Tarazaga, and Paul E. Plassmann. A multi-sensor stochastic energy-based vibro-localization technique with byzantine sensor elimination. *Sensors*, 23(23), 2023. ISSN 1424-8220. doi: 10.3390/s23239309. URL https://www.mdpi.com/1424-8220/23/23/9309.

[8] Murat Ambarkutuk, Sa'ed Alajlouni, Pablo A. Tarazaga, and Paul E. Plassmann. A multi-sensor stochastic energy-based vibro-localization technique with byzantine sensor elimination. *Sensors*, 23(23), 2023. ISSN 1424-8220. doi: 10.3390/s23239309. URL https://www.mdpi.com/1424-8220/23/23/9309.

[9] Ambarkutuk Murat and Tarazaga Pablo. Uncertainty analysis of an occupant localization technique based on simulated structural vibrations. In *IMAC-XL (40th) - 2022 A Conference and Exposition on Structural Dynamics*, Orlanda, Florida, USA, 2022. Society for Experimental Mechanics (SEM).

[10] R. Bahroun, O. Michel, F. Frassati, M. Carmona, and J. L. Lacoume. New algorithm for footstep localization using seismic sensors in an indoor environment. *Journal of Sound and Vibration*, 333:1046–1066, 2 2014. ISSN 0022460X. doi: 10.1016/j.jsv.2013.10.004.

[11] Jonathan Baker, Pablo Tarazaga, et al. Maximum likelihood estimation for passive energy-based footstep localization. *Mechanical Systems and Signal Processing*, 163:108158, 2022.

[12] Burçin Becerik-Gerber, Gale Lucas, Ashrant Aryal, Mohamad Awada, Mario Berges, Sarah L Billington, Olga Boric-Lubecke, Ali Ghahramani, Arsalan Heydarian, Farrokh Jazizadeh, et al. Ten questions concerning human-building interaction research for improving the quality of life. *Building and Environment*, 226:109681, 2022.

[13] Chiara Bedon. Body com acceleration for rapid analysis of gait variability and pedestrian effects on structures. *BUILDINGS*, 12(2), FEB 2022. doi: 10.3390/buildings12020251.

[14] Zhangjie Chen and Ya S Wang. Occupancy-driven smart register for building energy saving (conference presentation). In *Active and Passive Smart Structures and Integrated Systems 2017*, volume 10164, pages 175–175. SPIE, 2017.

[15] F. Ciampa and M. Meo. Acoustic emission source localization and velocity determination of the fundamental mode a0 using wavelet analysis and a newton-based optimization technique. *Smart Materials and Structures*, 19, 2010. ISSN 09641726. doi: 10.1088/0964-1726/19/4/045027.

[16] Jose Clemente, Fangyu Li, Maria Valero, and Wenzhan Song. Smart seismic sensing for indoor fall detection, location, and notification. *IEEE Journal of Biomedical and Health Informatics*, 24:524–532, 2 2020. ISSN 21682208. doi: 10.1109/JBHI.2019.2907498.

[17] Benjamin T. Davis, Juan M. Caicedo, and Victor A. Hirth. Force estimation and event localization (feel) of impacts using structural vibrations. *Journal of Engineering Mechanics*, 147, 3 2021. ISSN 0733-9399. doi: 10.1061/(asce)em.1943-7889.0001890.

[18] Benjamin T Davis, Brianna I Bryant, Stacy L Fritz, Reed Handlery, Alicia Flach, and Victor A Hirth. Measuring gait parameters from structural vibrations, 2022.

[19] Benjamin Thomas Davis. Characterization of human-induced vibrations characterization of human-induced vibrations. ISSN 10165077. URL https://scholarcommons.sc.edu/etd/3770.

[20] Yiwen Dong and Hae Young Noh. Ubiquitous gait analysis through footstep-induced floor vibrations. *SENSORS*, 24(8), APR 2024. doi: 10.3390/s24082496.

[21] Yiwen Dong, Joanna Jiaqi Zou, Jingxiao Liu, Jonathon Fagert, Mostafa Mirshekari, Linda Lowes, Megan Iammarino, Pei Zhang, and Hae Young Noh. Md-vibe: physics-informed analysis of patient-induced structural vibration data for monitoring gait health in individuals with muscular dystrophy. In *Adjunct Proceedings of the 2020 ACM International Joint Conference on Pervasive and Ubiquitous Computing and Proceedings of the 2020 ACM International Symposium on Wearable Computers*, UbiComp/ISWC '20 Adjunct, page 525–531, New York, NY, USA, 2020. Association for Computing Machinery. ISBN 9781450380768. doi: 10.1145/3410530.3414610. URL https://doi.org/10.1145/3410530.3414610.

[22] Yiwen Dong, Megan Iammarino, Jingxiao Liu, Jesse Codling, Jonathon Fagert, Mostafa Mirshekari, Meta Linda Lowes, Pei Zhang, and Anonymous Author. Ambient floor vibration sensing advances accessibility of functional gait assessment for children with muscular dystrophies. 2023. doi: 10.21203/rs.3.rs-3249615/v1. URL https://doi.org/10.21203/rs.3.rs-3249615/v1.

[23] Slah Drira and Ian F.C. Smith. A framework for occupancy detection and tracking using floor-vibration signals. *Mechanical Systems and Signal Processing*, 168, 4 2022. ISSN 10961216. doi: 10.1016/j.ymssp.2021.108472.

[24] Jonathon Fagert, Mostafa Mirshekari, Shijia Pan, Pei Zhang, and Hae Young Noh. Characterizing left-right gait balance using footstep-induced structural vibrations. volume 10168, page 1016819. SPIE, 4 2017. ISBN 9781510608214. doi: 10.1117/12.2260376.

[25] Jonathon Fagert, Mostafa Mirshekari, Shijia Pan, Linda Lowes, Megan Iammarino, Pei Zhang, Hae Young Noh, Dept of Civil, Environmental Engineering, Carnegie Mellon Univ, Forbes Ave, Postdoctoral Researcher, Stanford Univ, Via Ortega, Assistant Professor, Dept of Computer Science, Univ of California, North Lake Rd, Principal Investigator, Abigail Wexner Research Institute at Nationwide Children, Research Physical Therapist, Associate Research Professor, Dept of Electrical, Computer Engineering, Nasa Research Park, Po Box, Moffett Field, and Associate Professor. Structure- and sampling-adaptive gait balance symmetry estimation using footstep-induced structural floor vibrations, 2021.

[26] Jonathon Fagert, Mostafa Mirshekari, Pei Zhang, and Hae Young Noh. Recur-

sive sparse representation for identifying multiple concurrent occupants using floor vibration sensing. *Proceedings of the ACM on Interactive, Mobile, Wearable and Ubiquitous Technologies*, 6, 3 2022. ISSN 24749567. doi: 10.1145/3517229.

[27] Martin A. Fischler and Robert C. Bolles. Random sample consensus. *Communications of the ACM*, 24:381–395, 6 1981. ISSN 0001-0782. doi: 10.1145/358669.358692. URL https://dl.acm.org/doi/10.1145/358669.358692.

[28] Ahmed Abdel Ghany, Bernard Uguen, and Dominique Lemur. A robustness comparison of measured narrowband csi vs rssi for iot localization. volume 2020-November. Institute of Electrical and Electronics Engineers Inc., 11 2020. ISBN 9781728194844. doi: 10.1109/VTC2020-Fall49728.2020.9348854.

[29] Daniel Gomez, Shirley Rietdyk, and Shirley J. Dyke. Spatio-temporal assessment of gait kinematics in vertical pedestrian-structure interaction. *Structures*, 31:1199–1206, 2021. ISSN 2352-0124. doi: https://doi.org/10.1016/j.istruc.2021.02.024. URL https://www.sciencedirect.com/science/article/pii/S2352012421001351.

[30] James Howard and William Hoff. Forecasting building occupancy using sensor network data. In *Proceedings of the 2nd international workshop on big data, streams and heterogeneous source mining: Algorithms, systems, programming models and applications*, pages 87–94, 2013.

[31] Zhizhang Hu, Yue Zhang, and Shijia Pan. Footstep-induced floor vibration dataset: Reusability and transferability analysis. pages 546–551. Association

for Computing Machinery, Inc, 11 2021. ISBN 9781450390972. doi: 10.1145/3485730.3494117.

[32] Ellis Kessler, Vijaya VN Sriram Malladi, and Pablo A. Tarazaga. Vibration-based gait analysis via instrumented buildings. *International Journal of Distributed Sensor Networks*, 15, 2019. ISSN 15501477. doi: 10.1177/1550147719881608.

[33] Ellis Kessler, Pablo A. Tarazaga, and Robin Queen. *Defining Groupings and Classification of Human Gait Using Correlation of Ground Reaction Force Measurements*, volume 2, pages 377–384. 2019. ISBN 9783319744209. doi: 10.1007/978-3-319-74421-6_50. URL http://link.springer.com/10.1007/978-3-319-74421-6_50.

[34] Young Min Kwon and Gul Agha. Passive localization: Large size sensor network localization based on environmental events. pages 3–14, 2008. ISBN 9780769531571. doi: 10.1109/IPSN.2008.55.

[35] Fangyu Li, Jose Clemente, Maria Valero, Zion Tse, Sheng Li, and Wen Zhan Song. Smart home monitoring system via footstep-induced vibrations. *IEEE Systems Journal*, 14:3383–3389, 9 2020. ISSN 19379234. doi: 10.1109/JSYST.2019.2937960.

[36] Teng Li, Jiali Li, Luyu Bo, and Zhenhua Tian. Generating multi-pixel thermal images through an acousto-thermal effect. In *ASME International Mechanical Engineering Congress and Exposition*, volume 86670, page V005T07A010. American Society of Mechanical Engineers, 2022.

[37] Teng Li, Jiali Li, Luyu Bo, Michael R Brooks, Yingshan Du, Bowen Cai, Zhe Pei, Liang Shen, Chuangchuang Sun, Jiangtao Cheng, et al. Airborne acoustic vortex end effector-based contactless, multi-mode, programmable control of object surfing. *Advanced Materials Technologies*, page 2400564, 2024.

[38] L De Marchi, A Marzani, N Speciale, and E Viola. A passive monitoring technique based on dispersion compensation to locate impacts in plate-like structures. *Smart Materials and Structures*, 20:035021, 3 2011. ISSN 0964-1726. doi: 10.1088/0964-1726/20/3/035021. URL https://iopscience.iop.org/article/10.1088/0964-1726/20/3/035021.

[39] Yohanna MejiaCruz, Jean Franco, Garrett Hainline, Stacy Fritz, Zhaoshuo Jiang, Juan M. Caicedo, Benjamin Davis, and Victor Hirth. Walking speed measurement technology: a review. *Current Geriatrics Reports*, 10:32–41, 1 2021. ISSN 2196-7865. doi: 10.1007/s13670-020-00349-z. URL https://link.springer.com/10.1007/s13670-020-00349-z.

[40] Yohanna MejiaCruz, Zhaoshuo Jiang, Juan M. Caicedo, and Jean M. Franco. Probabilistic force estimation and event localization (pfeel) algorithm. *Engineering Structures*, 252, 2 2022. ISSN 18737323. doi: 10.1016/j.engstruct.2021.113535.

[41] Yohanna MejiaCruz, Juan M. Caicedo, Zhaoshuo Jiang, and Jean M. Franco. Probabilistic detection of impacts using the pfeel algorithm with a gaussian process regression model. *Engineering Structures*, 291:116255, 2023. ISSN 0141-

0296. doi: https://doi.org/10.1016/j.engstruct.2023.116255. URL https://www.sciencedirect.com/science/article/pii/S0141029623006703.

[42] Yohanna MejiaCruz, Juan M. Caicedo, Zhaoshuo Jiang, and Jean M. Franco. Probabilistic estimation of cadence and walking speed from floor vibrations. *IEEE Journal of Translational Engineering in Health and Medicine*, 12:508–519, 2024. ISSN 2168-2372. doi: 10.1109/JTEHM.2024.3415412.

[43] Mostafa Mirshekari, Shijia Pan, Pei Zhang, and Hae Young Noh. Characterizing wave propagation to improve indoor step-level person localization using floor vibration. volume 9803, page 980305. SPIE, 4 2016. ISBN 9781510600447. doi: 10.1117/12.2222136.

[44] Mostafa Mirshekari, Shijia Pan, Jonathon Fagert, Eve M. Schooler, Pei Zhang, and Hae Young Noh. Occupant localization using footstep-induced structural vibration. *Mechanical Systems and Signal Processing*, 112:77–97, 11 2018. ISSN 10961216. doi: 10.1016/j.ymssp.2018.04.026.

[45] Mostafa Mirshekari, Shijia Pan, Jonathon Fagert, Eve M Schooler, Pei Zhang, and Hae Young Noh. Occupant localization using footstep-induced structural vibration. *Mechanical Systems and Signal Processing*, 112:77–97, 2018.

[46] Mostafa Mirshekari, Jonathon Fagert, Shijia Pan, Pei Zhang, and Hae Young Noh. Step-level occupant detection across different structures through footstep-induced floor vibration using model transfer. *Journal of Engineering Mechanics*, 146, 3 2020. ISSN 0733-9399. doi: 10.1061/(asce)em.1943-7889.0001719.

[47] Mostafa Mirshekari, Jonathon Fagert, Shijia Pan, Pei Zhang, and Hae Young Noh. Obstruction-invariant occupant localization using footstep-induced structural vibrations. *Mechanical Systems and Signal Processing*, 153, 5 2021. ISSN 10961216. doi: 10.1016/j.ymssp.2020.107499.

[48] Ahmed Mohammed and Aleksandar Pavic. Human-structure dynamic interaction between building floors and walking occupants in vertical direction. *Mechanical Systems and Signal Processing*, 147, 1 2021. ISSN 10961216. doi: 10.1016/j.ymssp.2020.107036.

[49] Thibault Nowakowski, Laurent Daudet, and Julien de Rosny. Localization of acoustic sensors from passive green's function estimation. *The Journal of the Acoustical Society of America*, 138:3010–3018, 11 2015. ISSN 0001-4966. doi: 10.1121/1.4934951.

[50] Sai G.S. Pai, Yves Reuland, Slah Drira, and Ian F.C. Smith. Is there a relationship between footstep-impact locations and measured signal characteristics? pages 62–65. Association for Computing Machinery, Inc, 11 2019. ISBN 9781450370073. doi: 10.1145/3360773.3360888.

[51] Shijia Pan, Ningning Wang, Yuqiu Qian, Irem Velibeyoglu, Hae Young Noh, and Pei Zhang. Indoor person identification through footstep induced structural vibration. pages 81–86. Association for Computing Machinery, 2 2015. ISBN 9781450333917. doi: 10.1145/2699343.2699364.

[52] Jeffrey D. Poston, R. Michael Buehrer, Americo G. Woolard, and Pablo A. Tarazaga. Indoor positioning from vibration localization in smart buildings.

pages 366–372. IEEE, 4 2016. ISBN 978-1-5090-2042-3. doi: 10.1109/PLANS.2016.7479722. URL http://ieeexplore.ieee.org/document/7479722/.

[53] Jeffrey D. Poston, R. Michael Buehrer, and Pablo A. Tarazaga. A framework for occupancy tracking in a building via structural dynamics sensing of footstep vibrations. *Frontiers in Built Environment*, 3, 11 2017. ISSN 22973362. doi: 10.3389/fbuil.2017.00065.

[54] V. Racic, A. Pavic, and J. M.W. Brownjohn. Experimental identification and analytical modelling of human walking forces: Literature review. *Journal of Sound and Vibration*, 326:1–49, 2009. ISSN 0022460X. doi: 10.1016/j.jsv.2009.04.020.

[55] Paula Tarrío, Ana M. Bernardos, and José R. Casar. An energy-efficient strategy for accurate distance estimation in wireless sensor networks. *Sensors (Switzerland)*, 12:15438–15466, 11 2012. ISSN 14248220. doi: 10.3390/s121115438.

[56] Christina Turley, Margarite Jacoby, Gregory Pavlak, and Gregor Henze. Development and evaluation of occupancy-aware hvac control for residential building energy efficiency and occupant comfort. *Energies*, 13(20):5396, 2020.

[57] Maria Valero, Fangyu Li, Liang Zhao, Chi Zhang, Jose Garrido, and Zhu Han. Vibration sensing-based human and infrastructure safety/health monitoring: A survey. *Digital Signal Processing*, 114:103037, 7 2021. ISSN 10512004. doi: 10.1016/j.dsp.2021.103037. URL https://linkinghub.elsevier.com/retrieve/pii/S1051200421000762.

[58] Americo G. Woolard and Pablo A. Tarazaga. Applications of dispersion compensation for indoor vibration event localization. *JVC/Journal of Vibration and Control*, 24:5108–5117, 11 2018. ISSN 17412986. doi: 10.1177/1077546317744997.

[59] Americo G. Woolard, V. V. N. Sriram Malladi, Sa'ed Alajlouni, and Pablo A. Tarazaga. Classification of event location using matched filters via on-floor accelerometers. volume 10168, page 101681A, 4 2017. doi: 10.1117/12.2260113. URL http://proceedings.spiedigitallibrary.org/proceeding.aspx?doi=10.1117/12.2260113.

[60] Kaishun Wu, Yandao Huang, Minghui Qiu, Zhenkan Peng, and Lu Wang. Toward device-free and user-independent fall detection using floor vibration. *ACM Transactions on Sensor Networks*, 19:1–20, 2 2023. ISSN 1550-4859. doi: 10.1145/3519302.

[61] Da Yan, Tianzhen Hong, Bing Dong, Ardeshir Mahdavi, Simona D'Oca, Isabella Gaetani, and Xiaohang Feng. Iea ebc annex 66: Definition and simulation of occupant behavior in buildings. *Energy and Buildings*, 156:258–270, 2017.

Appendices

Appendix A

Theorems

Theorem A.1 (Rayleigh's Signal Energy Theorem)**.** *The Rayleigh's energy theorem states that the energy of a time domain continous and deterministic signal $y(t)$ is the integral of the square of magnitude of the signal. Equivalently, energy of the same signal can be obtained from its frequency-domain representation $Y(\omega)$.*

$$e = \int_{-\infty}^{\infty} |y(t)|^2 \, \mathrm{d}t = \int_{-\infty}^{\infty} |Y(\omega)|^2 \, \mathrm{d}\omega \tag{A.1}$$

Equivalently, the signal energy of a discrete time signal $y[k]$ is given by:

$$e = \sum_{k=-\infty}^{\infty} |y[k]|^2 = \sum_{k=-\infty}^{\infty} |Y(\omega_k)|^2 \tag{A.2}$$

Theorem A.2. *Squared sum of n number of nonstandard normally distributed random variables with unit variance follows the Noncentral Chi-squared distribution.*

Let $(X_1, \ldots, X_n)$ be normally distributed indepedent normal random variables with means $\mu_i \neq 0$ and unit variances $\sigma_i^2 = 1$ for $i = \{1, \ldots, n\}$. Let Y be the squared sum of the random variables X_i as shown in the equation below.

$$Y = \sum_{i=1}^{n} X_i^2 \sim \chi_n'^2(\lambda) \tag{A.3}$$

The resulting random variable Y is said to follow Noncentral Chi-squared distribution which denoted as $\chi_n'^2(\lambda)$. In the short hand representation $\chi_n'^2(\lambda)$, n represents the number of random variables used in the summation and is called degrees-of-freedom of the distribution, while $\lambda = \sum_{i=1}^{n} \mu_i^2$ represents the noncentrality parameter.

Theorem A.3. *Noncentral Chi-squared distribution converges to Normal distribution when n or λ is large.*

$$Y \sim \chi_n'^2(\lambda) \simeq \mathcal{N}(n+\lambda, 2n+4\lambda) \tag{A.4}$$

Theorem A.4 (Density Transformation Theorem)**.** *The density of functions of random variables can be calculated with the density transformation theorem. This theorem is essentially an extension of integration by substitution method.*

Let $\mathbf{X} = (X_1, \dots X_m)^\top \in \mathbb{R}^m$ be an m-dimensional multivariate random variable with a joint CDF of $F_{\mathbf{X}}(\mathbf{x}) = \mathrm{P}(\mathbf{X} \leq \mathbf{x})$ and joint PDF of $f_{\mathbf{X}}(\mathbf{x}) = \dfrac{\partial}{\partial x_1} \cdots \dfrac{\partial}{\partial x_m} F_{\mathbf{X}}(\mathbf{x})$. Assume $\mathbf{Y} = (Y_1, \dots Y_n)^\top \in \mathbb{R}^n$ is another multivariate random variable defined as a function of $\mathbf{X}$, $\mathbf{Y} = (g_1(\mathbf{X}) \dots g_n(\mathbf{X}))^\top = \mathbf{G}(\mathbf{X})$, where $g_i : (\mathbb{X}_1, \dots, \mathbb{X}_m) \subset \mathbb{R}^m \mapsto \mathbb{Y}_i \subset \mathbb{R}$ is an invertible multivariate continuous function.

By the virtue of the relation between PDF, we can show:

$$\int_{\mathbb{Y}_1} \cdots \int_{\mathbb{Y}_n} f_{\mathbf{Y}}(\mathbf{y}) \, \mathrm{d}y_1 \dots \mathrm{d}y_n = \int_{\mathbb{X}_1} \cdots \int_{\mathbb{X}_m} f_{\mathbf{X}}(\mathbf{x}) \, \mathrm{d}x_1 \dots \mathrm{d}x_m = 1 \tag{A.5a}$$

Thus, PDF of random variable $\mathbf{Y}$ *can be obtained as given below:*

$$f_{\mathbf{Y}}(\mathbf{y}) = \frac{\partial}{\partial y_1} \cdots \frac{\partial}{\partial y_n} \int_{\mathbb{X}_1} \cdots \int_{\mathbb{X}_m} f_{\mathbf{X}}(\mathbf{x}) \, \mathrm{d}x_1 \ldots \mathrm{d}x_m \tag{A.5b}$$

On the other hand, the CDF of random variable $\mathbf{Y}$*, can be shown as:*

$$F_{\mathbf{Y}}(\mathbf{y}) = \mathrm{P}(\mathbf{Y} \leq \mathbf{y}) = \mathrm{P}\left(\mathbf{X} \leq \mathbf{G}^{-1}(\mathbf{y})\right) \tag{A.6a}$$

$$F_{\mathbf{Y}}(\mathbf{y}) = \int_{\mathbf{s}}^{\mathbf{y}} f_{\mathbf{Y}}(\mathbf{y}) \, \mathrm{d}\mathbf{y} = \int_{\mathbf{G}^{-1}(\mathbf{s})}^{\mathbf{G}^{-1}(\mathbf{y})} f_{\mathbf{X}}(\mathbf{x}) \, \mathrm{d}\mathbf{x} \tag{A.6b}$$

where $\mathbf{s} = (\sup \mathbb{X}_1, \ldots, \sup \mathbb{X}_m)^\top$.

Now substitute $\mathbf{x} = \mathbf{G}^{-1}(\mathbf{u})$ *in the integral on the right hand side, i.e.,* $\mathbf{x} = \mathbf{G}^{-1}(\mathbf{u})$ *and* $\frac{\mathrm{d}\mathbf{u}}{\mathrm{d}\mathbf{x}} = \mathbf{G}'(\mathbf{x})$*. Due to the inverse function theorem, we also have* $\frac{\mathrm{d}\mathbf{x}}{\mathrm{d}\mathbf{u}} = \frac{\mathrm{d}\mathbf{G}^{-1}}{\mathrm{d}\mathbf{u}}$*. Consequentially,*

$$\int_{\mathbf{s}}^{\mathbf{y}} f_{\mathbf{Y}}(\mathbf{y}) \, \mathrm{d}\mathbf{y} = \int_{\mathbf{s}}^{\mathbf{y}} f_{\mathbf{X}}\left(\mathbf{G}^{-1}(\mathbf{u})\right) \frac{\mathrm{d}\mathbf{G}^{-1}}{\mathrm{d}\mathbf{u}} \, \mathrm{d}\mathbf{u} \tag{A.7a}$$

Taking the derivative of both sides with respect to $\mathbf{y}$*, we have:*

$$f_{\mathbf{Y}}(\mathbf{y}) = f_{\mathbf{X}}\left(\mathbf{G}^{-1}(\mathbf{y})\right) \frac{\mathrm{d}\mathbf{G}^{-1}}{\mathrm{d}\mathbf{y}} \tag{A.7b}$$

$$= f_{\mathbf{X}}\left(\mathbf{G}^{-1}(\mathbf{y})\right) \left|\det \mathbf{J}_{\mathbf{G}^{-1}}(\mathbf{y})\right| \tag{A.7c}$$

where $\mathbf{J}_{\mathbf{G}^{-1}}(\mathbf{y})$ *denotes the jacobian matrix of the inverse function* $\mathbf{G}^{-1}$ *evaluated at* $\mathbf{y}$*. Due to the implication of inverse function theorem and the properties of deter-*

minant operator, we have $|\det \mathbf{J}_{\mathbf{G}^{-1}}(\mathbf{y})| = |\det \operatorname{inv} \mathbf{J}_{\mathbf{G}}(\mathbf{y})| = \dfrac{1}{|\det \mathbf{J}_{\mathbf{G}}(\mathbf{x})|}$*, assuming* $\det \mathbf{J}_{\mathbf{G}}(\mathbf{x}) \neq 0$*, i.e.,* $\mathbf{G}(\mathbf{x})$ *is continuously differentiable.*

$$f_{\mathbf{Y}}(\mathbf{y}) = \frac{f_{\mathbf{X}}\left(\mathbf{G}^{-1}(\mathbf{y})\right)}{|\det \mathbf{J}_{\mathbf{G}}(\mathbf{x})|} \tag{A.7d}$$